Early spring subglacial discharge plumes fuel under-ice primary production at a Svalbard tidewater glacier

Tobias Reiner Vonnahme[1], Emma Persson[1], Ulrike Dietrich[1], Eva Hejdukova[2], Christine Dybwad[1], Josef Elster[3], Melissa Chierici[4,5], Rolf Gradinger[1]

[1] Department of Arctic and Marine Biology, UiT – The Arctic University of Norway, Tromsø, Norway
[2] Department of Ecology, Faculty of Science, Charles University, Prague, Czech Republic
[3] University of South Bohemia, České Budějovice, and Institute of Botany ASCR, Třeboň, Czech Republic
[4] Institute of Marine Research, Tromsø, Norway
[5] University Centre in Svalbard (UNIS), Longyearbyen, Svalbard, Norway

Correspondence to: Tobias R. Vonnahme (T.r.vonnahme@gmail.com)

Abstract. Subglacial upwelling of nutrient-rich bottom water is known to sustain elevated summer primary production in tidewater glacier influenced fjord systems. However, during the early spring season, the importance of subglacial upwelling has not been considered yet. We hypothesized that subglacial discharge under sea ice is present in early spring and that its flux is sufficient to increase phytoplankton primary productivity. We evaluated the effects of the submarine discharge on primary production in a seasonally fast-ice-covered Svalbard fjord (Billefjorden) influenced by a tidewater outlet glacier in April/May 2019. We found clear evidence for subglacial discharge and upwelling. Although the estimated bottom water entrainment factor (1.6) and total fluxes were lower than in summer studies, we still observed substantial impact on the fjord ecosystem and primary production at this time of the year. The subglacial discharge leads to a salinity stratified surface water layer and sea ice formation with low bulk salinity and permeability. The combination of the stratified surface layer, a two-fold higher under-ice irradiance due to a thinner snow cover, and higher N and Si concentrations at the glacier front supported two orders of magnitude higher phytoplankton primary production (42.6 mg C m^{-2} d^{-1}) compared to a marine reference site at the fast ice edge. Reciprocal transplant experiments showed that nutrient supply increased phytoplankton primary production by approximately 30 %. The brackish-water sea ice at the glacier front with its low bulk salinity contained a reduced brine volume, limiting the inhabitable brine channel space and nutrient exchange with the underlying seawater compared to full marine sea ice. Microbial and algal communities were substantially different in subglacial influenced water and sea ice compared to the marine reference site, sharing taxa with the subglacial outflow water. We suggest that with climate change, the retreat of tidewater glaciers in early spring could lead to decreased under-ice phytoplankton primary production. In contrast, sea ice algae production and biomass may become increasingly important, unless sea ice disappears before, in which case spring phytoplankton primary production may increase.

1 Introduction

Tidewater glacier fronts have recently been recognized as hotspots for marine production including top trophic levels, such as marine mammals, birds and piscivorous fish (Lydersen et al., 2014, Meire et al., 2016b), but also primary producers (Meire et al., 2016b, Hopwood et al., 2020). During summer, large amounts of freshwater are released below the glacier and entrap nutrient-rich bottom water, sediments and zooplankton during the rise to the surface (Lydersen et al., 2014, Meire et al., 2016a). Together with katabatic winds pushing the surface water out of the fjords, subglacial discharge creates a strong upwelling effect (Meire et al., 2016a). The biological response to this upwelling will depend on the characteristics of the upwelled water. Primary production and biomass is typically low (e.g. 0.6 ± 0.3 mg Chl a m^{-3}, Halbach et al., 2019) in direct proximity to the glacier front (within hundreds of meters to kilometres from the glacier front, Halbach et al., 2019) due to high sediment loads of the plumes absorbing light, but also due to lateral advection and the time needed for algae growth (Meire et al., 2016a,b, Halbach et al., 2019). The light absorbing effect of the plumes is highly dependent on the glacial bedrock type (Halbach et al., 2019). The high nutrient concentrations supplied to the surface can increase summer primary production at some distance (more than hundreds of meters to kilometres away from the glacier front, Halbach et al., 2019) from the initial discharge event, once the sediments settled out and algae had time to grow (Meire et al., 2016, Halbach et al., 2019). These tidewater upwelling effects have been described in a variety of different Arctic fjords including deep glacier termini in western Greenland (Meire et al., 2016a,b), eastern Greenland (Cape et al., 2019), and north-western Greenland (Kanna et al., 2018), but also in shallower fjords on Svalbard (Halbach et al., 2019). Due to the challenges of Arctic fieldwork in early spring and the difficulties of locating such an outflow, only few studies investigated subglacial discharge during that time window. The few studies available suggest an overall low discharge flux (e.g., Fransson et al., 2020, Schaffer et al., 2020) compared to summer values. However, the limited amount of data makes the generalized quantification of spring subglacial outflow difficult. In addition, studies focusing on the potential impacts of the early spring discharge on both sea ice and pelagic primary production are lacking.

In addition to submarine discharge at the grounding line, tidewater glacier related upwelling mechanisms can also be caused by the melting of deep icebergs (Moon et al., 2018), or the melting of the glacier terminus in contact with warm seawater (Moon et al., 2018, Sutherland et al., 2019). A seasonal study within an east Greenland fjord showed high melt rates of icebergs throughout the year, while subglacial runoff had been detected as early as April (Moon et al., 2018). However, freshwater inputs were generally substantially higher in summer (Moon et al., 2018). Glacier terminus melt rates of basal ice at the glacier-marine interface are low compared to the subglacial outflow flux but can be present throughout the year (Chandler et al., 2013, Moon et al., 2018). In fact, Moon et al. (2018) found higher basal iceberg melt rates below 200 m in winter compared to summer. The freshwater flux from these icebergs exceeds summer river runoff and reaches values of early summer (June-July) subglacial discharge (Moon et al., 2018), which may allow winter upwelling. Submarine glacier termini on Svalbard occur typically at shallower water depths than on Greenland and deep basal melt at the glacier terminus (below 200 m) and iceberg induced upwelling are less important (Dowdeswell, 1989). However, subglacial outflows can persist through winter and into

67   spring through the release of subglacial meltwater stored from the previous melt season (Hodgkins, 1997). Hodgkins (1997)

68   described the release of subglacial meltwater stored from the previous summer to fall melt season from various Svalbard

69   glaciers. Winter drainage occurred mostly periodically during events of ice-dam breakage in the subglacial drainage system.

70   During the storage period, the meltwater changes its chemical composition. During prolonged contact with silicon-rich

71   bedrock, the meltwater becomes enriched in the macronutrient silicate (Hodgkins, 1997). During freezing of the meltwater,

72   solutes are expelled leading to higher ion concentrations in the liquid fraction (Hodgkins, 1997). Under polythermal glaciers,

73   various other mechanisms such as constant freshwater supply from groundwater, and basal ice melt via geothermal heat,

74   pressure, or frictional dissipation can also be a continuous, but low flux meltwater source in winter and spring (Schoof et al.,

75   2014). Sediment inputs during this time of the year are low with peaks deeper in the water column, indicating limited impacts

76   on surface primary production (Moskalik et al., 2018). While studies on glacial discharge in winter and spring are limited to

77   oceanographic observations (Fransson et al., 2020, Schaffer et al., 2020), the biological effects on primary production have

78   been neglected (Chandler et al., 2013, Moon et al., 2018). We hypothesize that subglacial discharge can lead to significantly

79   increased primary production, due to upwelling of nutrient-rich deeper water or through its own nutrient load, especially

80   towards the end of the spring bloom. At the same time, considerably less light absorbing sediments are entrapped due to lower

81   upwelling fluxes compared to summer (Moskalik et al., 2018). After light becomes available in spring, ice algae and

82   phytoplankton may start forming blooms fuelled by nutrients supplied via winter mixing with different onsets in different parts

83   of the Arctic. The blooms are typically terminated by limitation of macronutrients, either nitrate or silicate (Leu et al., 2015).

84   We suggest that in the absence of wind-induced mixing, due to the seasonal presence of a fast ice cover in spring, submarine

85   discharge of glacial meltwater can directly (nutrient and ion enrichment over the subglacial storage period) or indirectly

86   (upwelling) be a significant source of inorganic nutrients. We suggest that these nutrients can significantly increase primary

87   production in front of tidewater glaciers compared to similar fjords without these glaciers especially after nutrients supplied

88   via winter mixing are used up (Leu et al., 2015). With climate change, these dynamics are expected to change substantially

89   (e.g., Błaszczyk et al., 2009, Holmes et al., 2019). Higher glacial melt rates and earlier runoff may initially increase tidewater

90   glacier induced upwelling, due to increased subglacial runoff (Amundson and Carroll, 2018). However, their retreat and

91   transformation into shallower tidewater glacier termini may lead to less pronounced upwelling, unless the shallower grounding

92   line is compensated by the increased runoff (Amundson and Carroll, 2018). Eventually, the tidewater glaciers transform into

93   land-terminating glaciers, where wind-induced mixing is still possible, but submarine discharge is eliminated (Amundson and

94   Carroll, 2018) – potentially reducing primary production.

95

96   Due to high inputs of freshwater in the autumn preceding the onset of sea ice formation, tidewater glacier influenced fjords are

97   often sea ice covered in spring, mainly by coastal fast ice. Within the sea ice, ice algae start growing, once sufficient light

98   penetrates the snow and ice layers between March and April, depending on latitude and local ice conditions (Leu et al., 2015).

99   While the beginning of the ice algal blooms is typically related to light, the magnitude depends on the initial nutrient

100   concentrations and advection of nutrient-rich seawater from the water column into the brine channel network (Gradinger,

101 2009). Thus, early spring subglacially induced upwelling has the strong potential to extend the duration and increase the

102 magnitude of the ice algal blooms. Similar control mechanisms apply to phytoplankton bloom formation and duration. Under-

103 ice phytoplankton blooms are thought to be light limited if the ice is snow covered and blooms have mostly been described in

104 areas with a lack of snow cover (e.g. melt ponds, after rain events, Fortier et al., 2002, Arrigo et al., 2014) or at the ice edge

105 related to wind-induced Ekman upwelling (Mundy et al., 2009). On Svalbard, low precipitation rates and strong katabatic

106 winds (Esau & Repina, 2012) often limit snow accumulation also on the fast ice near glacier fronts (Braaten, 1997), potentially

107 allowing enough light for under-ice phytoplankton blooms to occur. After sufficient light reaches the water column, typically

108 a diatom-dominated bloom starts along the receding ice edge or even below the sea ice (e.g., Hodal et al., 2012, Lowry et al.,

109 2017). Once silicate becomes limiting for diatom growth, other taxa like *Phaeocystis pouchetii* dominate the next stage of the

110 seasonal succession (von Quillfeldt, 2000). This succession pattern can be significantly influenced by tidewater glacier induced

111 spring upwelling. Sea ice formed from brackish water has relatively low bulk salinity, low brine volume, and low total ice

112 algal biomass as observed, for example, in the Baltic Sea (Haecky & Andersson, 1999). Sea ice with reduced bulk salinity has

113 a reduced permeability compared to more saline ice at identical temperatures (Golden et al., 1998). Brackish ice conditions

114 with low algal biomass will reduce light absorption allowing more light to reach the water column potentially fuelling under-

115 ice phytoplankton blooms. We suggest that even though subglacial upwelling is diminished in the spring, compared to the

116 summer, in the absence of wind mixing, the enriched nutrient concentrations may enhance algal growth at this time of year.

117

118 We used the natural conditions in a Svalbard fjord as a model system contrasting the biological response at two glacier fronts.

119 Only one of the glacier fronts supplies submarine freshwater discharge during the winter/spring (early spring) transition period

120 while a fast ice cover was present. In contrast, the other glacier front is mostly land-terminating. The aim of the study was to

121 investigate the effect of the glacier terminus, and subglacial outflow related upwelling on the light and nutrient regime in the

122 fjord and thereby on early spring primary productivity and algae community structures both in and under the sea ice. We

123 hypothesized that: 1) submarine discharge throughout winter and spring supplies nutrient-rich glacial meltwater and upwelling

124 of marine bottom water to the surface, 2) subglacial discharge increases primary production near the glacier front (< 500 m),

125 3) biomass of sea ice algae is lower at glacier fronts as a result of low permeability sea ice limiting nutrient exchange and

126 inhabitable space.

127 2 Methods

128 2.1 Field work and physical properties

129 Fieldwork was conducted on Svalbard in Billefjorden (Fig. 1) between 22nd of April and 5th of May 2019, when most samples

130 were collected. For comparison, some samples had been already taken in April 2018 (seawater, sea ice, and subglacial outflow

131 water for DNA analyses) and July 2018 (glacier ice and supraglacial runoff). Billefjorden is fed by a few streams, rivers and

132 the tidewater glacier Nordenskiöldbreen and is partly fast ice covered from January to June. Nordenskiöldbreen has an

133 estimated grounding depth of 20 m at its southern margin (CastAway CTD cast at the glacier front, data not shown). Tidal

134 currents are very slow with under 0.1 cm s^{-1}, which translates to advection below 22 m per tidal cycle (Kowalik et al., 2015).

135 Katabatic winds can be strong due to several glaciers and valleys leading into the fjord system (Láska et al., 2012). Together

136 with low precipitation, this leads to a thin snow depth on the sea ice. Bare sea ice spots are often present in the sea ice season

137 (personal observations). The fjord is separated from Isfjorden, a larger fjord connected to the West Spitsbergen current, by a

138 shallow approximately 30 to 40 m sill (Norwegian Polar Institute, 2020) making Billefjorden an Arctic fjord with limited

139 impacts of Atlantic water inflows. This character is shown in water masses, circulation patterns and animal communities

140 including the presence of polar cod (Maes, 2017, Skogseth et al., 2020).

141 Samples were taken at three stations: 1) at the fast ice edge (IE) – a full marine reference station (78°39'09N, 16°34'01E); 2)

142 at the southern site of the ocean-terminated glacier terminus (SG) (approx. 20 m water depth) with freshwater outflow observed

143 during the sampling period (78°39'03N, 16°56'44E) and; 3) at the northern site of the glacier terminus (NG) with no clear

144 freshwater outflow observed and a mostly land-terminating glacier front (78°39'40N, 16°56'19E).

145 Snow depth and sea ice thickness around the sampling area were measured with a ruler. Sea ice and glacier ice samples were

146 taken with a Mark II ice corer with an inner diameter of 9 cm (Kovacs Enterprise, Roseburg, OR, USA). Temperature of each

147 ice core was measured immediately by inserting a temperature probe (TD20, VWR, Radnor, PA, USA) into 3 mm thick pre-

148 drilled holes. For further measurements the ice cores were sectioned into the following sections: 0–3 cm, 3–10 cm and

149 thereafter in 20 cm long pieces from the bottom to the top, packed in sterile bags (Whirl-Pak™, Madison, WI, USA) and left

150 to melt at about 4–15 ˚C for about 24–48 h in the dark. Sections for chlorophyll *a* (Chl) measurements, DNA extractions, and

151 algae and bacteria counts were melted in 50 % vol/vol sterile filtered (0.2 µm Sterivex filter, Sigma-Aldrich, St. Louis, MO,

152 USA) seawater to avoid osmotic shock of cells (Garrison and Buck, 1986), while no seawater was added to the sections for

153 salinity and nutrient measurements. Salinity was measured immediately after melting using a conductivity sensor (YSI Pro 30,

154 YSI, USA). Brine salinity and brine volume fractions were calculated after Cox et al. (1983) for sea ice temperatures below -

155 2 °C and after Leppäranta and Manninen (1988) for sea ice temperatures above -2 °C.

156 Samples of under-ice water were taken using a pooter (Southwood and Henderson, 2000) connected to a hand-held vacuum

157 pump (PFL050010, Scientific & Chemical Supplies Ltd., UK). Deeper water at 1 m, 15 m, 25 m depths and bottom water at

158 the IE station were taken with a water sampler (Ruttner sampler, 2 L capacity, Hydro-Bios, Germany). Glacial outflow water

159 was sampled in April 2018 close to the SG station using sterile Whirl-Pak™ bags. No outflow water was found around the NG

160 station. Cryoconite hole water (avoiding any sediment) was sampled in July 2018 with a pooter on sites known to differ in

161 their biogeochemical settings (Nordenskiöldbreen main cryoconite site (NC), and Nordenskiöldbreen near Retrettøya (NR)

162 sites characterized by Vonnahme et al., 2016). One-metre long glacier surface ice samples were taken with the Mark II ice

163 corer at the southern side of the glacier on the NC site.

164 CTD profiles were taken at each station by a CastAway™ (SonTek/-Xylem, San Diego, CA, USA). At the SG station an

165 additional CTD profile was taken with a SAIV CTD SD208 (SAIV, Lakselv, Norway) including turbidity and fluorescence

166 sensors. Unfortunately, readings at the other stations failed due to sensor freezing at low air temperatures. Surface light data

167 were obtained from the photosynthetic active radiation (PAR) sensor of the ASW 1 weather station in Petuniabukta (23 m

168 a.s.l), operated by the University of South Bohemia (Láska et al., 2012, Ambrožová and Láska, 2017).

169 During the sampling days, Billefjorden was overcast. The light regime under the ice was calculated after Masicotte et al. (2018)

170 with a snow albedo of 0.78, a snow attenuation coefficient of 15 m^{-1} (Mundy et al., 2005), ice attenuation coefficients of 5.6

171 m^{-1} for the upper 15 cm and 0.6 m^{-1} below (Perovich et al., 1998). For sea ice algae, an absorption coefficient of 0.0025 m^2

172 (mg Chl)$^{-1}$ was used. The fraction of fjord water versus subglacial meltwater for the water samples was calculated assuming

173 linear mixing (Equations 1-2) of the two salinities (glacial meltwater salinity = 0 PSU, average seawater salinity at IE=34.7 $\pm$

174 0.03 standard deviation), since no other water masses in regard to temperature or salinity signature were present (Table 1). The

175 variability of the IE seawater salinity leads to a small (< 1%) uncertainty in the estimated value of the relative contributions of

176 sea water vs subglacial meltwater.

2.2 Chemical properties

178 Nutrient samples of water and melted sea ice and glacier ice were sterile filtered as described above, stored in 50 ml falcon

179 tubes (which were acid washed in 5 % vol/vol HCl and MQ rinsed) and kept at -20 °C until processing. Total alkalinity (TA),

180 Dissolved inorganic carbon (DIC), and pH samples were sampled in 500 ml borosilicate glass bottles avoiding air

181 contamination and fixed within 24 h with 2 % (final conc.) $HgCl_2$ and stored at 4 °C until processing.

182 Nutrients were measured in triplicates using standard colorimetric methods with a nutrient autoanalyser (QuAAtro 39, SEAL

183 Analytical, Germany) using the instrument protocols: Q-068-05 Rev. 12 for nitrate and nitrite (detection limit = 0.02 µmol L^{-1}

184 ^{1}), Q-066-05 Rev. 5 for silicate (detection limit = 0.07 µmol L^{-1}), and Q-064-05 Rev. 8 for phosphate (detection limit = 0.01

185 µmol L^{-1}). The data were analysed using the software AACE v5.48.3 (SEAL Analytical, Germany). Reference seawater (Ocean

186 Scientific International Ltd., United Kingdom) was used as blanks for calibrating the nutrient analyser. The maximum

187 differences between the measured triplicates were 0.1 µmol L^{-1} for silicate and nitrate and 0.05 µmol L^{-1} for nitrite and

188 phosphate. Concentrations of nitrate and nitrite (NO_X) were used to estimate the fraction of bottom water reaching the surface

189 at SG assuming linear mixing of subglacial meltwater, bottom water (at station IE) and surface water concentration using the

190 NO_X concentration measured at IE and the subglacial meltwater (Table 1). The calculations for these mixing estimates are

191 given in the appendix (Equations 3-6).

192 DIC and TA were analyzed within 6 months after sampling as described by Jones et al. (2019) and Dickson et al. (2007). DIC

193 was measured on a Versatile Instrument for the Determination of Titration carbonate (VINDTA 3C, Marianda, Germany),

194 following acidification, gas extraction, coulometric titration, and photometry. TA was measured with potentiometric titrations

195 in a closed cell on VINDTA Versatile INstrument for the Determination of Titration Alkalinity, VINDTA 3S, Marianda,

196 Germany). Precision and accuracy was ensured via measurements of Certified Reference Materials (CRM, obtained from

197 Dickson, Scripps Institution of Oceanography, USA). Triplicate analyses on CRM samples showed mean standard deviations

198 below ± 1 µmol kg^{-1} for DIC and TA.

2.3 Biomass and communities

For determination of algal pigment concentrations, about 500 ml of seawater or melted sea ice were filtered onto GF/F filter (Whatman plc, Maidstone, UK) in triplicates using a vacuum pump (max 200 mbar vacuum) before storing the filter in the dark at -20 °C. Water and melted sea ice for DNA samples were filtered onto Sterivex filter (0.2 µm pore size) using a peristaltic pump and stored at -20 °C until extraction. Algae were sampled in two ways; 1) a phytoplankton net (10 µm mesh size) was pulled up from 25 m and the samples fixed in 2 % (final conc.) neutral Lugol and stored at 4 °C in brown borosilicate glass bottles before processing; and 2) water or melted sea ice was fixed and stored directly as described above. For later bacteria abundance estimation, 25 ml of water was fixed with 2 % (final conc.) formaldehyde for 24–48 h at 4 °C before filtering onto 0.2 µm polycarbonate filters (Isopore™, Merck, US) and washing with filtered seawater and 100 % ethanol before freezing at -20 °C.

Algal pigments (Chl *a*, phaeophytin) were extracted in 5 ml 96 % ethanol at 4 °C for 24 h in the dark. The extracts were measured on a Turner Trilogy AU-10 fluorometer (Turner Designs, 2019) before and after acidification with a drop of 5 % HCl. 96 % ethanol was used as a blank and the fluorometer was calibrated using a chlorophyll standard (Sigma S6144). For estimations of algae derived carbon, a conversion factor of 30 g C (g Chl)$^{-1}$ was applied (Cloern et al., 1995). The maximum differences (max-min) between the measured triplicates were under 0.05 µg Chl L^{-1} unless stated otherwise.

DNA was isolated from the Sterivex filter cut out of the cartridge using sterile pliers and scalpels, using the DNeasy® PowerSoil® Kit following the kit instructions with a few modifications. Solution C1 was replaced with 600 µL Phenol:Chloroform:Isoamyl Alcohol 25:24:1 and washing with C2 and C3 was replaced with two washing steps using 850 µL chloroform. Before the last centrifugation step, the column was incubated at 55 °C for 5 min to increase the yield. For microbial community composition analysis, we amplified the V4 region of a ca. 292 bp fragment of the 16S rRNA gene using the primers (515F, GTGCCAGCMGCCGCGGTAA and 806R, GGACTACHVGGGTWTCTAAT, assessed by Parada et al., 2016). For eukaryotic community composition analyses, we amplified the V7 region of ca 100-110 bp fragments of the 18S rRNA gene using the primers (Forward 5'-TTTGTCTGSTTAATTSCG-3' and Reverse 5'-GCAATAACAGGTCTGTG-3', assessed by Guardiola et al., 2015). The Illumina MiSeq PE library was prepared after Wangensteen et al. (2018).

For qualitative counting of algal communities, the phytoplankton net and bottom sea-ice samples were counted under an inverted microscope (Zeiss Primovert, Carl Zeiss AG, Germany) with 10x40 magnification. For quantitative counts, 10-50 ml of the fixed water samples were settled in an Utermöhl chamber (Utermöhl, 1958) and counted. Algae were identified using identification literature by Tomas (1997), and Throndsen et al. (2007). For bacteria abundance estimates, bacteria on polycarbonate filter samples were stained with DAPI (4,6-diamidino-2-phenylindole) as described by Porter and Feig (1980), incubating the filter in 30 µl DAPI (1 µg ml^{-1}) for 5 min in the dark before washing with MQ and ethanol and embedding in Citifluor:Vectashield (4:1) onto a microscopic slide. The stained bacteria were counted using an epifluorescence microscope (Leica DM LB2, Leica Microsystems, Germany) under UV light at 10x100 magnification. At least 10 grids or 200 cells were counted. The community structure of the phytoplankton net haul was used for estimating the contribution of sea ice algae to

232   the settling community based on typical Arctic phytoplankton (Von Quillfeldt, 2000) and sea ice algal species (von Quillfeldt

233   et al., 2003) described in literature.

2.4 In situ measurements and incubations

235   Vertical algal pigment fluxes were measured using custom made (Faculty of Science, Charles University, Prague, Czech

236   Republic) short-term sediment traps (6.2 cm inner diameter, 44.5 cm height) at 1 m, 15 m, and 25 m under the sea ice anchored

237   to the ice at SG and IE, as described by Wiedmann et al. (2016). Sediment traps were left for 24 h at the SG station and 37 h

238   at the IE station. After recovery, samples for algal pigments were taken, fixed and analysed as described above. Vertical export

239   fluxes were calculated as described in equation 7.

240   Primary production (PP) was measured based on ^{14}C-DIC incorporation. Samples were incubated *in situ* in 100 ml polyethylene

241   bottles attached to the rig of the sediment trap giving identical incubation times. Seawater or bottom sea ice melted in filtered

242   seawater (ca 20 °C initial temperature to ensure fast ice melt) on site were incubated with ^{14}C sodium bicarbonate at final

243   concentration of 1 µCi ml^{-1} (PerkinElmer Inc., Waltham, USA). PP samples were incubated in triplicates for each treatment

244   with two dark controls for the same times as the sediment traps. Samples were filtered onto precombusted Whatman GF/F

245   filters (max 200 mbar vacuum) and acidified with a drop of 37 % fuming HCl for 24 h for removing remaining inorganic

246   carbon. The samples were measured in the Ultima Gold™ Scintillation cocktail on a liquid scintillation counter (PerkinElmer

247   Inc., Waltham, USA, Tri-Carb 2900TR) and PP was calculated after Parsons et al. (1984). Dark carbon fixation (DCF) rates

248   were used to estimate bacterial biomass production using a conversion factor of 190 mol POC (mol CO_2)$^{-1}$ fixed (Molari et al.,

249   2013).

250   For testing the effect of the water chemistry on phytoplankton growth, we designed a reciprocal transplant experiment where

251   the phytoplankton communities at SG and IE (1 m and 15 m) were transplanted into the sterile filtered water of both SG and

252   IE. 50 ml of the water containing the phytoplankton communities of SG or IE were transferred into 50 ml sterile filtered (0.2

253   µm) seawater of SG or IE in 100 ml polyethylene bottles. The bottles with IE communities were then incubated under the ice

254   at the IE station and the SG communities under the ice at the SG station. The aim of the experiment is to test if water chemistry

255   alone is sufficient to increase primary production, or if the different communities, light regimes, or temperatures are more

256   important. These samples were incubated and processed together with the other PP incubations at the respective depths as

257   described above.

2.5 Statistics and bioinformatics

259   Silicate, phosphate and NO_X concentrations were plotted against salinities and tested for correlations via linear regression

260   analysis using the lm function in R (R Core Team, Vienna, Austria). P values were corrected for multiple testing using the

261   false discovery rate. Since the primary production estimates of the reciprocal transplant experiments were not normally

262   distributed, came from a nested design, and had heterogeneous variance, a robust nested Analysis of variance (ANOVA) was

263   performed to test for significant treatment effects of incubation water with water depth as nested variable.

264 16S sequences were analysed using a pipeline modified after Atienza et al. (2020) based on OBITools v1.01.22 (Boyer et al.,

265 2014). The raw reads were demultiplexed and trimmed to a median phred quality score minimum of 40 and sequence lengths

266 between 215 bp and 299 bp (16S rRNA) or between 90 bp and 150 bp (18S rRNA) and merged. Chimaeras were removed

267 using uchime with a minimum score of 0.9. The remaining merged sequences were clustered using swarm (Mahe et al., 2014).

268 16S swarms were classified using the RDP classifier (Wang et al., 2007) and 18S swarms using the sina aligner (Pruesse et

269 al., 2012) with the silva SSU 138.1 database (Quast et al., 2012). Further multivariate analyses were done in R using the vegan

270 package. The non-metric multidimensional scaling (NMDS) plots are based on Bray-Curtis dissimilarities of square root

271 transformed and double Wisconsin standardized OTU tables and were used to visualize differences between groups (brackish

272 water at SG – Fjord water, sea ice – seawater). Analysis of Similarities (ANOSIM) were done to test for differences of the

273 communities between the groups (999 permutations, Bray-Curtis dissimilarities).

274 **3 Results**

275 **3.1 Physical parameters**

276 The physical conditions of sea ice (temperature T/bulk salinity S, Fig. 2a,b) and surface water (uppermost 4 m under the sea

277 ice, T and S, Fig. 2c,d) at the freshwater inflow impacted site SG differed substantially from NG and IE. The sea ice and the

278 upper 4 m under the sea ice had consistently lower salinities (<8 PSU) and higher temperatures (-0.4 ˚C to -0.2 ˚C) at SG

279 compared to NG and IE and also compared to the deeper water masses at SG (salinity > 34.6 PSU, temperature < -1.4 ˚C)(Fig.

280 2c,d). Sea ice melt was unlikely because the measured water temperatures and sea ice temperatures were below the freezing

281 point considering the sea ice bulk salinity. The water column at SG was highly stratified with a low salinity 4 m thick layer

282 under the sea ice, separated by a sharp ca 1 m thick pycnocline (Fig. 2c,d). In contrast, the water column at IE was fully mixed

283 and at NG only a minor salinity drop from 34.6 to 33.6 PSU occurred within the upper 50 cm under the sea ice (Fig. 2c,d). Sea

284 ice temperature and salinity showed similar variations between the three sites with SG ice having lower salinities and higher

285 temperatures relative to sea ice at the other stations (Fig. 2a,b). At SG, bulk salinities were mostly below 0.7 PSU and calculated

286 brine salinities below 14 PSU, except for the uppermost 20 cm where bulk salinities reached around 1.7 PSU and a brine

287 salinity of 32 PSU (Fig. 2). This resulted in very low brine volume fractions below 5 %, except for the lowermost 10 cm with

288 brine volume fractions up to 9 % (Supplementary table S1). At IE and NG, bulk salinities are mostly above 5 PSU (>40 PSU

289 brine salinity) and temperatures were below -0.4 ˚C, which led to brine volume fractions above 6 % in all samples and above

290 10 % in the bottom 30 cm.

291 The homogenous temperature and salinity water column profiles at IE and NG stations indicate the presence of only one water

292 mass (Local Arctic water, Skogseth et al., 2020). The only additional water mass was subglacial meltwater (salinity of 0 PSU)

293 mixed into the surface layer of SG. Applying a simple mixing model based on the two salinities (IE= 34.7 PSU, Glacier= 0

294 PSU) provided an estimation of the fraction of glacially derived water in the surface layer of ca. 85 % in the uppermost 2 m

295 under the sea ice, before decreasing to 0 % at 4 m under the sea ice below the strong halocline. The water sample taken 1 m

296 under the sea ice had a fraction of 32 % glacial meltwater (Table 1). For NG, glacial derived water contributed only 3 % in the

297 first 50 cm under the sea ice.

298 The SG station was 33 m deep and about 180 m away from the glacier front. The sea ice was 1.33 m thick and covered by 3

299 cm of snow. The ice appeared clear with some minor sediment and air bubble inclusions and missed a skeletal bottom layer.

300 In the water column, a higher potential sediment load was observed as a turbidity peak at the halocline (Fig. 3). Direct evidence

301 of subglacial outflow had been observed at the southern site of the glacier in form of icing and liquid water flowing onto the

302 sea ice in April 2018, April 2019 and October 2019 (Fig. S4), but this form of subglacial outflow froze before reaching the

303 fjord, which was additionally blocked by impermeable sea ice. The sea ice temperature was between -0.4 ˚C at the bottom and

304 -1.7 ˚C at the top (Fig. 2b).

305 NG was 27 m deep and about 360 m away from the glacier front. The sea ice was thinner (0.92 m) and the snow cover thicker

306 (6 cm) compared to SG. The ice had a well-developed skeletal layer at the bottom with brown coloration due to algal biomass.

307 The ice temperature ranged between -2 ˚C at the bottom to -2.7 ˚C at the top (Fig. 2b). The IE station was about 75 m deep

308 and 50 m away from the ice edge. The sea ice was thinnest (0.79 m) and the snow cover thickest (10 cm). Sea ice temperatures

309 were coldest ranging from -2.2 ˚C at the bottom to -3.1 ˚C on the top (Fig. 2b). Loosely floating ice algae aggregates were

310 present in the water directly under the ice. The recorded surface PAR irradiance were similar during the primary production

311 incubation times at SG and IE (SG: average=305 μE m^{-2} s^{-1}, min=13 μE m^{-2} s^{-1}, max=789 μE m^{-2} s^{-1}; IE: average=341 μE m^{-2}

312 s^{-1}, min=37 μE m^{-2} s^{-1}, max=909 μE m^{-2} s^{-1}). Using published attenuation coefficients irradiance directly under the ice was 5

313 μE m^{-2} s^{-1} at IE and with 9 μE m^{-2} s^{-1} higher at SG due to the thinner snow cover.

3.2 Nutrient variability in sea ice and water

315 Subglacial outflow water and glacial ice had relatively low nutrient levels (in glacial ice: $Si(OH)_4$ < 0.3 μmol L^{-1}, NO_X < 0.9

316 μmol L^{-1}, PO_4 < 0.75 μmol L^{-1}, in outflow: $Si(OH)_4$ <1.5- 2.0 μmol L^{-1}, NO_X 1.8- 2.3 μmol L^{-1}, PO_4 < 0.1 μmol L^{-1}), but the

317 nutrient concentrations in subglacial outflow water were higher than in most sea ice samples and the depleted surface water (1

318 m under the sea ice) at the IE. Nutrient concentrations in the fjord were highest in the bottom water (4.0- 4.5 μmol L^{-1} $Si(OH)_4$,

319 9.1- 9.6 μmol L^{-1} NO_X, 0.7-0.8 μmol L^{-1} PO_4) and depleted at the surface and in the sea ice with the exception of the under-

320 ice water (UIW, 0- 1 cm under the sea ice) of SG, where NO_X (10 μmol L^{-1}) and silicate (19 μmol L^{-1}) levels were exceptionally

321 high (Fig. 4). We cannot exclude anomalies or sampling artifacts to be responsible for the high UIW values, and therefore used

322 the values measured 1 m under the sea ice for further calculations in this manuscript as surface water reference. SG had overall

323 higher levels of silicate and NO_X compared to the IE at both 1 m below the sea ice (factors of 3 for $Si(OH)_4$ and 2 for NO_X)

324 and bottom ice (factor of 18 for $Si(OH)_4$ and 3 for NO_X compared to IE bottom ice) (Fig. 4). Silicate concentrations deeper in

325 the water column were similar at all the stations with values of ca 4 μmol L^{-1} . Close to the surface silicate was reduced to 1.6

326 μmol L^{-1} at 1 m at the IE, while it stayed at 4.3 μmol L^{-1} at SG (Fig. 4a). In the water column, NO_X and phosphate gradients

327 were similar between the sites. However in sea ice, NO_X concentrations were more than two times higher at SG than at the IE.

328 In the bottom 30 cm of sea ice all nutrients had higher concentrations at SG, except for phosphate, which was depleted in the

10

329 bottom 3 cm of SG, but not in the bottom of IE sea ice. In the ice interior at 50- 70 cm distance from the ice bottom, also the

330 other nutrients were depleted at SG, before rising slightly towards the surface of the ice. N:P ratios were generally highest at

331 SG with values above 40, exceeding Redfield ratios in the surface water and sea ice. N:P ratios at the IE were below Redfield

332 in the entire water column and bottom sea ice with values ranging from 10 to 13. A slight increase in NO_X was observed at the

333 sea ice-atmosphere interface at NG and SG.

334 Nutrient versus salinity profiles can give indications of the endmembers (sources) of the nutrients (Fig. 5) with a linear

335 correlation being indicative of conservative mixing. A positive correlation indicates higher concentrations of the nutrients of

336 the saline Atlantic water endmember, while a negative correlation points to a higher concentration in the fresh glacial meltwater

337 endmember. Biological uptake and remineralisation could weaken or eliminate the correlation, indicating non-conservative

338 mixing. In the water column at NG and IE silicate (R^2=0.66, p=0.008), NO_X (R^2=0.62, p=0.01) and phosphate (R^2=0.69,

339 p=0.005) showed conservative positive mixing patterns with higher contributions of Atlantic water (Fig. 5a-c). SG showed a

340 negative correlation for silicate pointing to a higher contribution of glacial meltwater (R^2=0.86, p<0.0001). The absence of

341 correlations for NO_X and PO_4 indicate non-conservative mixing pointing towards the relevance of biological uptake and release

342 (Fig. 5d-f). At SG, silicate concentrations were higher with lower salinities. The same pattern was observed in sea ice, with

343 higher silicate and NO_X concentrations in the fresher SG ice, compared to NG and IE (Fig. 5g-i). However, the R^2 value were

344 lower in particular for $Si(OH)_4$ (NO_X: R^2=0.18, p=0.059; $Si(OH)_4$: R^2=0.41, p=0.002).

345 The contribution of nutrients by upwelling as well as freshwater inflow from glacial meltwater at SG was estimated by linear

346 mixing calculations for 1 m below the sea ice, avoiding the potential outlier values directly under the ice (Equations 1-6). At

347 1 m below the sea ice, about 32 ±0.1 % of the water was derived from glacial meltwater based on salinity-based mixing of

348 glacial meltwater and local Arctic water (Table 1, Eq. 1-2). The remaining 68 % came from either bottom water upwelling (25

349 m at SG as reference) or surface water (IE values at 1 m under the sea ice as reference). Inorganic nutrients behaved

350 conservatively at the IE reference (Fig. 5a-c), which allows similar mixing calculation of the bottom water fraction. Based on

351 linear mixing of inorganic nutrients, 58 ±1 % of NO_X and 49 ±3 % of PO_4 was provided by subglacial upwelling (Table 1).

352 For silicate, higher concentrations were required in the bottom water of subglacial meltwater at the glacier front to explain the

353 very high surface concentrations measured. Considering the estimated NO_X and PO_4 fractions, the overall fraction of nutrients

354 derived from upwelling was about 53 %. The overall budget 1 m under the sea ice was 32 ±0.1 % glacial meltwater, 53 ±3 %

355 subglacial upwelling (marine bottom water), and 15 ±3 % horizontal transport (surface water).

356 **3.3 Carbon cycle**

357 Net primary productivity (NPP) was overall one order of magnitude higher at SG than at IE, with the highest production value

358 occurring within the brackish layer under the ice at SG (5.27 mg m^{-3} d^{-1}, Fig. 6, 7). Within this layer, also Chl values were

359 about two times higher compared to IE (21 mg m^{-3} at SG, 9.1 mg m^{-3} at IE), and also the Chl-specific productivity in this layer

360 exceeded values at the other stations (Table 2). Within sea ice, a slightly different pattern emerged. While the primary

361 productivity in the bottom sea ice (0–3 cm) was two times higher at SG compared to IE, Chl values were two orders of

362 magnitude lower (Fig. 6). This indicates high Chl-specific production at SG (5.6 mg C mg Chl d^{-1} in the sea ice and 11.4 mg

363 C mg Chl d^{-1} integrated over 25 m depth). At the IE, the contribution of released ice algae to algal biomass in the water column

364 was higher and the overall vertical Chl flux was about 1.5 times higher than at SG at 25 m depth. Bacterial biomass was

365 comparable at both stations with higher biomass concentrations within the ice than in the water column. Bacterial activity

366 (based on DCF) was comparable in the bottom sea ice at the two sites; however, it was 63x higher in the brackish surface water

367 of SG leading to very high growth rate estimates (Table 2) of 6 mg C m^{-3} d^{-1}. Due to a conversion factor from a very different

368 habitat (Molari et al., 2013), the absolute bacterial growth rate estimates are likely overestimations.

369 Integrated Chl values over the uppermost 25 m of the water column were nearly identical for SG and IE with values of about

370 3.75 mg Chl m^{-2} (Table 2). The fraction of Chl was highest at IE (85 %) and lowest at the SG (30 %) (Table 2). The integrated

371 NPP was considerably higher at SG (42.6 mg C m^{-2} d^{-1} at SG, 0.2 mg C m^{-2} d^{-1} at IE), while the vertical export of Chl was

372 about three times higher at IE than SG. This leads to more (14 times) vertical export based on the sediment trap measurements

373 than production at IE and considerably lower (5 %) export than production at SG (Table 2). Relative to the standing stock

374 biomass of Chl at IE, 0.2 % of the Chl was renewed daily by NPP at IE and 3 % was vertically exported daily at IE, which

375 would relate - assuming absence of advection – to a daily loss of 3 % of the standing stock Chl. At SG, 38 % was renewed per

376 day, while 2 % were exported. As grazing was not estimated in this study, the suggested loss terms of Chl based on the sediment

377 trap data are likely underestimations. This leads to an accumulation of biomass of 38 % per day, and a doubling time of about

378 2.6 days. Bacterial growth doubling times were estimated to be between minutes (SG water) and days (IE water), but within

379 hours in sea ice (Table 2).

380 Considering the N demand based on the carbon based PP measurement (16 mol C mol N^{-1} after Redfield, 1934), about 2 μmol

381 N L^{-1} month^{-1} (equivalent to 32 % of 1 m value for NO$_X$) was needed to sustain the PP measured at SG. Assuming constant PP

382 and steady state nutrient conditions, 32 % of the surface water had to be replaced by subglacial upwelling per month to supply

383 this N demand via upwelling. Since only 62 % of the upwelling water was entrained bottom water the actual vertical water

384 replenishment rate would be 52 % per month. Assuming a 2 m freshwater layer under the ice, this translates to flux of about

385 1.1 m^3 m^{-2} month^{-1}. Considering a distance of 250 m to the glacier front and a width of 1.6 km of the SG bay, this translates to

386 a minimum of about 422,000 m^3 month^{-1}.

387 The reciprocal transplant experiment aimed to show the effect of water chemistry on primary production in the absence of

388 effects related to different communities, temperature, or light. The results (Fig. 7) showed clearly that the higher NPP at SG,

389 compared to NG was related to the nutrient concentrations (nested ANOVA, p=0.0038, F=10.88). In any combination, sterile

390 filtered water from the SG had a fertilising effect on both SG and IE communities, increasing PP of IE communities by approx.

391 30 %. SG communities of the most active fresh surface layer (1 m) fixed twice as much CO$_2$ when incubated in the same water,

392 compared to incubations in the IE water.

3.4 Bacterial, archaeal and eukaryotic communities

After bioinformatic processing 13,043 bacterial and archaeal (16S rRNA) OTUs, belonging to 1,208 genera with between 9,708 and 331,809 reads were retained. Differences between the bacterial 16S sequences of the various sample types indicated that they can be used as potential markers for the origin of the water (Fig. 8). Sea ice and water communities are clearly separated (ANOSIM, p=0.004, R=0.35) with no overlapping samples (Fig. 8a). Generally IE and NG communities were very similar, while sea ice and under-ice water communities at SG were significantly different (ANOSIM, p=0.001, R=0.593) from the other fjord samples. The NMDS showed also separation of 16S communities along a gradient from subglacial communities towards fjord communities, with SG communities being in between fjord and subglacial communities (Fig. 8a). Bacterial communities at SG in the bottom layer of the sea ice and the brackish water layer were more similar to subglacial outflow communities than the other samples in both 2018 and 2019. Six OTUs were unique to the glacial outflow and SG surface (closest relatives: *Fluviimonas*, *Corynebacterineae*, *Micrococcinae*, *Hymenobacter*, *Dolosigranuum*), which are 6.6 % of their OTUs. The community structure of supraglacial ice was very different from any other sample. Also in the most abundant genera clear differences can be detected (Fig. S1). *Flavobacterium* sp. was most abundant in sea ice and UIW samples in both 2018 and 2019 at SG, but rare or absent in the other samples. *Aliiglaciecola* sp. was characteristic for NG sea ice and UIW samples. *Paraglaciecola* sp. was abundant in NG and IE sea ice and UIW samples, and *Colwellia* sp. was abundant in all sea ice and UIW samples. In seawater samples the genus *Amphritea* sp. was more abundant. *Pelagibacter* sp. was abundant in all samples. Glacial outflow water was dominated by *Sphingomonas* sp. and glacier ice by *Halomonas* sp., which were rare or absent in the other samples.

The eukaryotic community (18S rRNA) consisted of 4,711 OTUs, belonging to 535 genera, with between 2,204 and 15,862 reads. Overall, the same NMDS clustering has been found as for the 16S rRNA sequencing. We found distinctive communities in the sea ice and 1 m layer under the sea ice at SG being significantly different (ANOSIM, p=0.001, R=0.456) to the other samples (Fig. 8c). In fact, the SG surface communities were more similar to the outflow community (Fig. 8c). The clear differentiation between all sea ice and water column communities was also visible in the 18S rRNA samples (ANOSIM, p=0.005, R=0.192). As for the 16S communities, also the abundant genera differed between the groups (Fig. S2). The cryptophytes *Hemiselmis* sp. and Geminigeraceae were abundant at SG, but rare at the other sites. Dinophyceae, Imbricatea (*Thaumatomastix* sp.) and Bacillariophyceae were abundant in all samples with diatoms being mostly more abundant in sea ice or UIW. The Chytridiomycota family of Lobulomycetaceae were abundant in water samples from 2018, but not 2019. Subglacial outflow water was dominated by unclassified Cercozoa and *Bodomorpha* sp..

In total 22 different taxa were detected by microscopy. The community composition was clearly separated between sea ice and water samples. Furthermore sea ice species composition at SG differed from NG and IE (Fig. 8c). SG sea ice was completely dominated by unidentified flagellates (potentially *Hemiselmis* sp., Geminigeraceae, and *Thaumatomastix* sp. based on 18S sequences), with the exception of the 70–90 cm layer with high abundances of *Leptocylindrus minimus*. Sea ice samples at NG and IE were dominated by the typical ice algae *Navicula* sp. and *Nitzschia frigida*. Water samples were more diverse with high

426　abundances of *Fragillariopsis* sp., *Coscinodiscus* sp., and *Chaetoceros* sp.. Overall, diatoms dominated most samples at NG

427　and IE in sea ice and water samples.

4 Discussion

429　The hydrography, sea ice properties, water chemistry and bacterial communities at SG provide clear evidence for submarine

430　discharge and upwelling at a shallow tidewater outlet glacier under sea ice, a system previously not considered for subglacial

431　upwelling processes. Briefly, our first hypothesis that submarine discharge persists also in early spring, supplying nutrient-

432　rich glacial meltwater and upwelling of bottom fjord water to the surface has been confirmed as discussed in detail below.

4.1 Indications for subglacial discharge and upwelling

434　The physical properties at SG were distinctly different to stations NG and IE. In contrast to NG and IE, the marine terminating

435　SG site had a brackish surface water layer of 4 m thickness under the sea ice and low sea ice bulk salinities below 0.7 PSU,

436　with the exception of the uppermost 20 cm with a bulk salinity of 1.7 PSU. The sea ice bulk salinity is comparable to sea ice

437　in the nearby tidewater glacier influenced Tempelfjorden (Fransson et al., 2020) and brackish Baltic sea ice (Granskog et al.,

438　2003). We excluded surface melt or river runoff as freshwater sources for the following reasons. With air temperatures below

439　freezing point during the sampling periods, surface runoff based on snowmelt was not possible and no melting was observed

440　during fieldwork. In addition, there are no major rivers known to flow into the main bay studied (Adolfbukta), due to the small

441　catchment areas (Norsk Polarinstitutt, 2020). We did observe some subglacial runoff at the southern site of the glacier (close

442　to SG), but this outflow water froze before it reached the fjord, which was additionally blocked by a 1.33 m thick sea ice cover.

443　The sea ice cover would also block any inputs by atmospheric precipitation, considering the impermeable sea ice conditions

444　especially at SG with brine volume fractions below 5 % (Golden et al., 1998, Fransson et al., 2020). If surface runoff was

445　present, we would also expect a similar pattern at the NG site. In fact, due to the closer proximity to the southward facing

446　mountains and higher sea ice permeability, NG would be more likely influenced by surface runoff than SG. Other potential

447　freshwater sources could be related to subaqueous melt of the glacier terminus, (Holmes et al., 2019, Sutherland et al., 2019),

448　icebergs (Moon et al., 2018), or ice melange (Mortensen et al., 2020). However, in the absence of Atlantic water inflow, which

449　is blocked by a shallow sill at the entrance of Billefjorden (Skogseth et al., 2020), water temperatures were consistently below

450　the freezing point (max -0.2 ˚C) and no Atlantic inflow water (Temperature $\geq$ 1 ˚C and Salinity $\geq$ 34.7 PSU, Skogseth et al.,

451　2020) was detected at any station. These low water temperatures do not allow glacier terminus ice to melt. Besides, Billefjorden

452　is not characterized by large amounts of icebergs or ice melange as described from Greenland glaciers (Moon et al., 2018;

453　Mortensen et al., 2020). However, glacier terminus ice melt is likely more important in systems with Atlantic water inflows,

454　such as Greenland or Svalbard fjords without a shallow sill (e.g. Kongsfjorden and Tunabreen, Holmes et al., 2019). Sea ice

455　may melt at lower temperatures compared to glacial ice, but the absence of typical sea ice algae in the water column at SG and

456　the low salinity of the sea ice indicated that this was not the case. In fact, sea ice with a salinity of 1.5 PSU (measured at SG)

457 would melt at -0.08 ˚C (Fofonoff et al., 1983), but the water and ice temperatures did not exceed -0.2 ˚C. In fact, at this
458 temperature the brackish surface water and meltwater of the submarine discharge would be supercooled. We did find a 1.5 cm
459 layer of frazil ice on the bottom of the SG sea ice showing that this did have some influence on sea ice formation. The subglacial
460 meltwater would need to introduce some heat, allowing the meltwater to reach the surface as liquid water. A temperature
461 maximum at the sea ice-water interface supports this hypothesis. This heat may also lead to basal sea ice melt adding
462 freshwater closer to the glacier front and main plume. However, sea ice melt as freshwater source cannot explain the low
463 salinity of the sea ice itself. Consistent with our study Fransson et al. (2020) also found substantial amount of freshwater in
464 the sea ice in Tempelfjorden (approx. 50 % meteoric water fraction) in a year with large glacier meltwater contribution further
465 supporting the presence of subglacial discharge under sea ice in our study. Fransson et al. (2020) suggested the combination
466 of low salinities with high silicate concentrations as indicator for glacial meltwater contributions, which was also the case in
467 our study. In addition, the overall low sea ice salinity and sediment inclusions at SG cannot be explained by sea ice melt, but
468 must originate from another source. Clear evidence for outflow comes also from the visual observations of subglacial outflow
469 exiting the land-terminating part south of the glacier in October 2019, April 2018 and April 2019, which we assume also
470 occurred under the marine-terminating front. In fact, subglacial outflows in spring is a common phenomenon observed at
471 various other Svalbard glaciers with runoff originating from meltwater stored under the glacier from the last melt season and
472 released by changes in hydrostatic pressure or glacier movements (Wadham et al., 2001). Active subglacial drainage systems
473 in winter have also been described elsewhere, and can be sustained by geothermal heat or frictional dissipation, groundwater
474 inputs, or temperate ice in the upper glacier (Wilson 2012, Schoof et al., 2014). This meltwater has also been found to be rich
475 in silicate due to the long contact with the subglacial bedrock during its storage over winter (Wadham et al., 2001, Fransson et
476 al., 2020). We therefore suggest that early spring subglacial discharge is not unique to Billefjorden, but likely occurs at all
477 polythermal or warm based marine-terminating glaciers.

478 **4.2 Potential magnitude of subglacial discharge and upwelling**

479 Considering the slow tidal currents in our study area (<22 m per 6 h tidal period, Kowalik et al., 2015) and wind mixing
480 blocked by sea ice, a potential source of the freshwater within Billefjorden may be meltwater introduced during the late summer
481 to fall melt season and remaining throughout winter. Hence, the question of how much subglacial meltwater reaches the surface
482 in what timeframe is important. We estimated that the surface water was most likely exchanged on time scales of days to
483 weeks. Even slow vertical mixing would be capable to erode the halocline in over six months since the last melt season. The
484 turbidity peak that we observed at the halocline would also settle out in a short time (weeks), if not replenished by fresh inputs
485 (Meslard et al., 2018). We determined vertical export flux to account for approximately 4% of the Chl standing stock at 25 m
486 (Table 2). Considering that glacial sediment settles typically much faster than phytoplankton due its higher density this suggests
487 that the turbidity peak would erode within days to weeks without fresh sediment inputs via upwelling (Meslard et al., 2018).

488 Furthermore, the inorganic nitrogen demand for the measured primary production would consume the present nutrients in a

489 few (approx. 2) months. Assuming steady state, the nutrient uptake by phytoplankton primary production would require an

490 upwelling driven water flux of at least 1.1 m^3 m^{-2} month^{-1}.

491 Microbial communities (16S rRNA and 18S rRNA) in SG UIW and sea ice were similar to the subglacial outflow water.

492 Bacterial communities (16S rRNA) at SG shared 6.6 % of their OTUs with subglacial outflow communities, which is twice as

493 much as NG and IE (3.6 %) shared with the outflow communities. Considering the estimated bacterial production and biomass

494 (Table 2) at SG the doubling time of the bacteria would be between 0.5 h and 7 h (Table 2). However, the use of a conversion

495 factor for biomass production based on sediment bacterial data is adding uncertainty to the estimation of the bacterial doubling

496 time. Estimates reported from Kongsfjorden in April are indeed longer (3-10 days, Iversen & Seuthe, 2010), as are other Arctic

497 bacterioplankton doubling time estimates ranging between 1.2 days (Rich et al., 1997), 2.8 days (de Kluijver et al., 2013) and

498 weeks (2 weeks, Rich et al., 1997, 1 week, Kirchman et al., 2005).

499 Based on the growth in the range of hours to days, the distinctive community at SG would have changed to a more marine

500 community on time scales of weeks, assuming only growth of marine OTUs at SG and settling out or grazing of inactive glacial

501 bacteria taxa. Thus, we suggest that the presence of shared OTUs between SG and the glacial outflow may indicate a continuous

502 supply of fresh inoculum to sustain these taxa.

503 The amount of discharge and upwelling was estimated using hydrographic data. In our study, three water masses were

504 distinguished; i) subglacial outflow (SGO) with low salinity (0 PSU) relatively high temperatures (>0 ˚C) and high silicate

505 concentrations (Cape et al., 2019), (ii) deep local Arctic water (DLAW) entrained from approx. 20 m with low temperatures

506 (-1.7 ˚C) high salinities (34.7 PSU) and high nutrient concentrations (Skogseth et al., 2020), and iii) surface local Arctic water

507 (SLAW) with the same temperature and salinity signature as the DLAW, but depleted in nutrients (Skogseth et al., 2020).

508 Nutrients were depleted in the UIW, but not at 15 m depth, showing that the nutricline was shallower than 15 m. Hence,

509 subglacial discharge at a glacier terminus depth of 20 m would be sufficient to cause upwelling of nutrient rich DLAW to the

510 surface. In fact, our mixing calculations (Equations 1-6) estimate that 32 % of the SG water 1 m under the sea ice was derived

511 by SGO, which pulled 1.6 times as much (53 % DLAW : 32 % SGO = ratio of 1.6) DLAW with it during upwelling. Fransson

512 et al. (2020) found that 30-60 % of glacier-derived meltwater was incorporated in the bottom sea ice at the glacier front of

513 Tempelfjorden, which is comparable to our study, again indicating that early spring subglacial discharge and the resulting

514 formation of sea ice with low porosity is a widespread process at marine terminating glacier fronts in Svalbard. Uncertainties

515 with these estimates may be related to sea ice melt as additional freshwater source, and to slightly different nutrient

516 concentrations directly in the SG subglacial discharge compared to the sampled subglacial outflow at some distance.

517 **4.3 Importance of subglacial discharge and upwelling under sea ice**

518 To our knowledge, our study provides currently the only available estimate of subglacial upwelling in early spring. Our study

519 suggests that subglacial upwelling in spring results in a small volume transport of only about 1.1 m^3 m^{-2} month^{-1} (approx. 2 m^3

520 s^{-1}) in Billefjorden. This estimate is based on the flux of nutrient rich bottom water needed to maintain the measured primary

production assuming steady state conditions and is therefore a rough, but conservative estimate. Due to logistical limitations, we could not sample the subglacial outflow directly at the SG site, but at some distance. Consequently, submarine discharge at SG may have slightly different nutrient concentrations due to potentially different bedrock chemistry. The most comparable estimate on the magnitude of the upwelling is available at Kronebreen for summer. This Svalbard tidewater glacier is of similar size and had one order of magnitude higher upwelling rates compared to our study (31-127 $m^3\ s^{-1}$, Halbach et al., 2019). Due to their size, summer subglacial upwelling flux in Greenland is two to four times higher than at Kronebreen (250-500 $m^3\ s^{-1}$, Carroll et al., 2016). In our study about 1.6 times as much bottom water from about 20 m (DLAW) as subglacial outflow water (SOW) reached the surface at SG (Entrainment factor of 1.6 – see above). The entrainment factor is mostly dependent on the depth of the glacier front (Carroll et al., 2016). In fact, the glacier terminus at SG was shallower (approx. 20 m) than any other studied tidewater glacier on Svalbard (70 m depth at Kronebreen, Halbach et al., 2019) or Greenland (> 100 m, Hopwood et al., 2020). Hence, the higher summer entrainment factors estimated in Kongsfjorden (3, Halbach et al., 2019) and Greenland (6 to 30, Hopwood et al., 2020) are not surprising. Glacier terminus depth appears to be the main control of entrainment rates, likely independent of the time of the year. However, turbulent mixing may cause increased entrainment during times of very high subglacial discharge rates. The higher entrainment factors in Greenland also lead to more saline water reaching the surface and the strongly stratified brackish surface layer observed at SG has not been observed at these deep tidewater glaciers (e.g., Mortensen et al., 2020). Kronebreen is the most comparable tidewater glacier in terms of glacier terminus depth and entrainment rate. Although the estimated entrainment factor was low at Kronebreen (3), subglacial upwelling substantially increased summer primary production in Kongsfjorden (Halbach et al., 2019). In spite of the shallow depth, and the low discharge and entrainment rate of our study, subglacial upwelling appears to be the main mechanism to replenish bottom water with high nutrient concentrations to the surface and can substantially increase spring primary production due to; (i) subglacial outflow below (approx. 20 m) the nutricline (<15 m), (ii) the absence of any other terrestrials inputs, (iii) Atlantic water blocked by a shallow sill (Skogseth et al., 2020), (iv) very weak tidal currents (Kowalik et al., 2015), (iv) wind mixing blocked by sea ice in Billefjorden, and (v) undiluted subglacial meltwater having lower nutrient concentrations than the DLAW.

4.4 Importance for under-ice phytoplankton

Our main finding was that i) higher irradiance, ii) a stratified surface layer, and iii) increased nutrient supply via subglacial discharge and upwelling allowed increased phytoplankton primary production at SG. The ice edge station (IE) was light and nutrient limited and supported a lower phytoplankton primary production.

4.4.1 Increased light

Despite the subglacial discharge and upwelling, the negative effect of light limitation with the massive sediment plumes in summer (Pavlov et al., 2019) were not observed in early spring. We did measure a small turbidity peak under the SG sea ice, but the values were comparable to open fjord systems in summer (Meslard et al., 2018, Pavlov et al., 2019), where light is sufficient for photosynthesis. Under-ice phytoplankton blooms are typically limited by light, which is attenuated and reflected

by the snow and sea ice cover (Fortier et al., 2002, Mundy et al., 2009, Ardyna et al., 2020). Some blooms have been observed, mostly under snow-free sea ice, such as after snow melt (Fortier et al., 2002), under melt ponds (Arrigo et al., 2012, Arrigo et al., 2014), after rain events (Fortier et al., 2002), or at the ice edge related to wind-induced Ekman upwelling (Mundy et al., 2009). In our study however, light levels available for phytoplankton growth were low compared to other under-ice phytoplankton bloom studies (Mundy et al., 2009, Arrigo et al., 2012), but higher at SG than at IE. This can be explained through the combined effects of sea ice and snow properties at SG. Light attenuation in low salinity sea ice is typically lower due to a lower brine volume (Arst and Sipelgas, 2004). Also, lower sea ice algae biomass and thinner snow cover due to snow removal with katabatic winds (e.g., Braaten 1997, Laska et al., 2012) leads to less light attenuation and a lower albedo. Our estimates showed that about twice as much light reached the water at SG compared to the IE, in spite of the thicker sea ice cover. The estimated light levels of 5 and 9 $\mu E\ m^{-2}\ s^{-1}$ were above the minimum irradiance (1 $\mu E\ m^{-2}\ s^{-1}$) required for primary production (Mock & Gradinger, 1999). Hence, the increased light under the brackish sea ice at SG could be one factor explaining the under-ice phytoplankton bloom observed.

4.4.2 Stratified surface layer

The strong stratification at SG is another factor; allowing phytoplankton to stay close to the surface, where light is available, allowing a bloom to form. In fact, Lowry et al. (2017) found that convective mixing by brine expulsion in refreezing leads can inhibit phytoplankton blooms even in areas with sufficient under-ice light and nutrients. At the same time, they found moderate phytoplankton blooms under snow covered sea ice (1–3 mg Chl m^{-3}) sustained by a more stratified surface layer, which was, however, still an order of magnitude lower than the SG values. Our finding of a higher vertical flux at IE compared to SG shows that stronger stratification may indeed be a contributing factor for the higher phytoplankton biomass at SG due to lower loss rate. However, our reciprocal transplant experiment clearly showed, that location alone (light, stratification) could not explain the increased primary production, but that the water properties at SG had a fertilising effect on algal growth, most probable because of higher nutrient levels, which were limiting at IE. In contrast to SG, higher plume entrainment factors at deep Greenland tidewater glaciers (Hopwood et al., 2020) lead to subglacial meltwater typically highly diluted with saline bottom water, once it reaches the surface, resulting in high salinities and a rather weak salinity driven stratification directly at the glacier front (Mortensen et al., 2020). Hence, the strong effect on stratification may be a unique feature of shallow tidewater glaciers.

4.4.3 Upwelling and meltwater influx of nutrients

Algal growth at IE was co-limited by lower irradiance as well as nutrient concentrations. Dissolved inorganic nitrogen (DIN) to phosphate ratios (N:P) at the IE were mostly below Redfield ratios (16:1), especially in sea ice with DIN concentrations below 1 $\mu mol\ L^{-1}$, indicating potential nitrogen limitations (Ptacnik et al., 2010), while the N:P ratio at SG was balanced and close to Redfield. Silicate concentrations below 2 $\mu mol\ L^{-1}$ are typically considered limiting for diatom growth (Egge & Aksnes, 1992) and this threshold had been reached at UIW and sea ice (concentration estimate in brine volume) at IE, but not

at SG. This indicates that nitrate supplied by bottom water upwelling and silicate by combined upwelling and additions from the glacial runoff had a fertilising effect on the SG water. High silicate values have also been observed at glacier fronts in other areas such as Greenland fjords (Azetsu-Scott and Syvitski, 1997) and Tempelfjorden (Fransson et al., 2015, 2020). Iron has not been measured, but is an essential micronutrient, often enriched in subglacial meltwater (Bhatia et al., 2013, Hopwood et al., 2020). However, iron limitation is untypical in coastal Arctic systems (Krisch et al., 2020). Besides the subglacial upwelling, nutrient concentrations may simply be higher due to less physical forcing and time needed for vertical mixing down to the bottom at the shallower water depth at SG compared to IE. However, NG was slightly shallower than SG and algal growth was still limited by nutrients. Besides, silicate and nitrate showed negative correlations with salinity, when including SG samples. In fact, these nutrients only correlated positively with salinity at IE and NG, while at SG, the negative correlations or non-conservative mixing are indicative for subglacial upwelling (mainly N and Si) and/or meltwater input (for Si) (Hopwood et al., 2020). Biological nutrient uptake did not play a significant role, due to relatively low bacterial and primary production. The subglacial outflow water itself was poor in nitrate, but high in silicate due to the interaction with the subglacial bedrock and long residence time below the glacier (Wadham et al., 2001), which was also found in Tempelfjorden (Fransson et al., 2015, 2020). Nordenskiöldbreen has a mix of metamorphic bedrock including silicon rich gneiss, amphibolite, and quartzite, but also carbonate rich marble (Strzelecki, 2011), which can partly contribute to the high silicate levels observed. The role of bedrock derived minerals and particles for composition of sea ice chemistry have been described in the neighbouring fjord (Tempelfjorden) in detail by Fransson et al. (2020). Silicate concentrations in subglacial outflow water were lower ($<1.5 - 2$ μmol L^{-1}) compared to estimates in Greenland (Meire et al., 2016a, Hawkings et al., 2017, Hatton et al., 2019), indicating that direct fertilisation in early spring may be even more important in other tidewater glacier influenced fjords. Another potential source may be higher silicate concentrations in the sediments at SG (Hawkings et al., 2017). While bottom water values were similar between SG and IE, high concentrations in the SG sediments themselves is a probable source not accounted for in the present study.

Another nitrogen source may be ammonium, which was introduced via subglacial upwelling in Kongsfjorden (Halbach et al., 2019). Ammonium regeneration and subsequent nitrification (Christman et al., 2011) under the sea ice, may explain the exceptionally high nitrate concentration of the UIW at SG, which can be part of the explanation for the high N:P ratios. In fact, bacterial activity was higher at SG potentially allowing higher ammonium recycling. Another explanation for the high N:P ratios and low phosphate concentrations can be related to phosphate scavenging by iron, as discussed by Cantoni et al. (2020). Nitrate can be supplied through the subglacial meltwater itself (Wynn et al., 2007), but we did not find high nitrate concentrations in the undiluted subglacial outflow water in our study. Atmospheric inputs of N have been shown in the Baltic Sea, but thinner sea ice and warm periods with increased sea ice permeability were needed for the N to reach the brine pockets or water column (Granskog et al., 2003). Our NO$_X$ profiles show some evidence of atmospheric N deposition, but only at NG and SG, which may be related to precipitation or surface flooding. For under-ice phytoplankton, these atmospheric N inputs play probably no role, but may have benefitted the high *Leptocylindrus* algae biomass layer in the upper ice parts of SG. Overall, the clearest evidence of nutrient limitations and fertilisation by subglacial discharge and upwelling was demonstrated

619 with the reciprocal transplant experiment, which showed an approx. 30 % increase in primary production of algae communities
620 incubated in SG water. Overall, primary production at SG was an order of magnitude higher than at IE. This indicates that
621 both fertilisation by submarine discharge and upwelling and increased light and stratification play a role in increasing
622 phytoplankton primary production.

623 4.4.4 Increased phytoplankton primary production

624 The integrated primary production to 25 m at SG was 42.6 mg C m^{-2} d^{-1} which is low compared to other marine-terminating
625 glacier influenced fjord systems in summer with integrated NPP of 480 ±403 mg C m^{-2} d^{-1} (Hopwood et al., 2020), including
626 studies in Kongsfjorden on Svalbard with 250 -900 mg C m^{-2} d^{-1} (Van de Poll et al., 2018). Also, studies conducted at the same
627 time (1 May) observed higher primary production rates in a marine-terminating glacier influenced fjord system, such as
628 Kongsfjorden (1520-1850 mg C m^{-2} d^{-1}, Hodal et al., 2012). However, none of these systems were sea ice covered during the
629 study periods and therefore not limited by light compared to our study. Under sea ice, phytoplankton communities have
630 typically much lower NPP rates of 20–310 mg C m^{-2} d^{-1} with only about 10 % or less light transmission reaching the water
631 column (Mundy et al., 2009). These values are more comparable to the SG values, despite the lower estimated light
632 transmission (3 %). In the central Arctic, higher under-ice NPP has been measured, but always related to high light transmission
633 due to the absence of ice, or under melt ponds with light transmissions up to 59 % (Arrigo et al., 2012). However, in the sea
634 ice area north of Svalbard, Assmy et al. (2017) found substantial spring PP below relatively thick sea ice of refrozen leads.
635 This was also confirmed by a large CO_2 decrease due to primary production under the sea ice (Fransson et al., 2017).
636 Phytoplankton production under snow-covered Arctic sea ice is often considered negligible compared to sea ice algae or
637 summer production. This can be shown in low biomass, mostly consisting of settling sea ice algae (Leu et al., 2015), or very
638 low NPP rates (e.g., Pabi et al., 2008). The same has been observed under Baltic sea ice with similar low light levels and
639 primary production between 0.1–5 mg C m^{-2} d^{-1} under snow-covered sea ice and about 30 mg C m^{-2} d^{-1} under snow-free sea
640 ice (Haecky & Andersson, 1999). These values are comparable to the IE without subglacial meltwater influence, but an order
641 of magnitude lower than the production at SG. Moderate blooms of 1–3 mg Chl m^{-3} have been described under snow-covered
642 sea ice with equal (3 %) light transmission (Lowry et al., 2017). Lowry et al. (2017) argues that a stratified water column and
643 sufficient nutrients allow moderate blooms even under these low light conditions. In particular, diatoms, the most common
644 taxa of under ice phytoplankton blooms (von Quillfeldt, 2000, this study) are known to be well adapted to low light conditions
645 (Furnas, 1990). Our study found Chl values up to an order of magnitude higher than Lowry et al. (2017), showing that under-
646 ice phytoplankton blooms are indeed important under snow-covered sea ice and can be facilitated by subglacial discharge and
647 upwelling.
648 Our study is the first to show that the combination of several factors (stratified water column, increased light and supply of
649 fresh nutrients via tidewater glacier driven processes) can support a rather productive under-ice phytoplankton community,
650 exceeding biomass and production of under-ice phytoplankton in systems with comparable light levels. Besides the increased
651 and extended primary production fuelled by tidewater glacier, the active and abundant phytoplankton taxa in surface water

652 with consistently replenished nutrients, may be a viable seed community for summer phytoplankton blooms, once the sea ice

653 disappears and light levels increase (Hegseth et al., 2019). The significantly different community at SG may also contribute to

654 an overall more diverse seed community available to the entire fjord, compared to fjords without early spring subglacial

655 discharge.

4.5 Impact on sea ice algae

4.5.1 Impact on biomass and primary production

658 While phytoplankton biomass and production were clearly increased at SG, exceeding levels of other snow-covered under-ice

659 systems, sea ice algal biomass and activity had been differently affected. Our third hypothesis suggested lower sea ice algae

660 biomass and production at SG due to the lower brine volume fractions. In agreement with our hypothesis, algal biomass was

661 indeed an order of magnitude lower compared to the IE and NG. However, primary production was two times higher, showing

662 more efficient photosynthesis.

663 Compared to most other sea ice studies conducted during the same period of the year, typically representing the mid-bloom

664 phase with 10–20 mg Chl m^{-2} (Leu et al., 2015), Chl biomass was very low at all stations of our study (<0.32 mg Chl m^{-2}).

665 Only Greenland fjords (0.1-3.3 mg Chl m^{-2}) or pre- and post-bloom systems had comparably low biomass (Mikkelsen et al.,

666 2008, Leu et al., 2015). The significantly different communities with a high number of cryptophyte flagellates, a high

667 proportion of phaeophytin (14–68 % in the bottom 3 cm), and a high contribution of sea ice algae in the water column indicate

668 that we sampled indeed a post-bloom situation. Considering the low air, sea ice and water temperatures and the absence of a

669 fresh UIW layer at the IE, the bloom was most likely not terminated by bottom ice erosion but by nutrient depletion. In fact,

670 SG bottom ice was deficient in phosphate (0.27 µmol (L brine)$^{-1}$), while IE was deficient in silicate (1 µmol (L brine)$^{-1}$) and

671 nitrogen (N:P = 1 mol N mol P^{-1}). This finding fits to earlier studies where phosphate limitations had been described as limiting

672 for brackish sea ice algae at concentrations below 0.27 µmol L^{-1} (Haecky and Andersson, 1999), while N and Si limitations

673 are typical for Arctic sea ice algae (Gradinger, 2009). The low concentrations of phosphate in the subglacial meltwater would

674 partly explain the low concentration in SG sea ice. In addition, most studies summarized by Leu et al. (2015) were done 10

675 years or more prior to our measurements. In fact, the Greenland study by Mikkelsen et al. (2008) with comparable sea ice algae

676 biomass had the thinnest sea ice cover of 0.5 m sampled in the warmest year (2006). During our study, the weather station in

677 Longyearbyen measured a mean temperature of –3.9 °C in April 2019, which was 8.3 °C above average and the second

678 warmest average April temperature recorded after April 2006 (0.1 °C), indicating that a warmer climate may explain the earlier

679 bloom termination (yr.no, 2020).

680 Similar to algal biomass, primary production (approx. 0.01 mg C m^{-2} d^{-1} at SG and 0.005 mg C m^{-2} d^{-1} at IE, assuming 10 cm

681 productive bottom layer) was considerably lower than in most studies of Arctic sea ice (0.8–55 mg C m^{-2} d^{-1} in the Barents

682 Sea) mentioned by Leu et al. (2015). Only studies on algal aggregates (Assmy et al., 2013) and Baltic sea ice (Haecky &

683   Andersson, 1999) measured similarly low production rates indicating that the senescence of the bloom (aggregates) and brine

684   volume fraction (Baltic Sea) were factors contributing to low primary production in sea ice.

4.5.2 Stressors in brackish sea ice

686   In addition to the post bloom status of the bloom, the lower biomass at SG can be partly explained by the lower brine salinity.

687   Permeability of sea ice is typically related to salinity and temperature, which determine the brine volume. With a brine volume

688   fraction below 5 %, or a temperature below -5 °C and a salinity below 5 PSU, sea ice is considered impermeable (Golden et

689   al., 1998). At SG, temperatures were higher, but a brine volume fraction above 5 % was only found in bottom ice sections (7–

690   9 %), indicating that the brine channels are weakly connected and algae had limited inhabitable place and nutrient supply

691   (Granskog et al., 2003), especially in the upper layers of the sea ice. In more saline systems, such as the Chukchi or Beaufort

692   Sea a high flux of seawater through the ice (0.4–19 m^3 seawater m^{-2} sea ice) has been discussed as crucial to allow continuous

693   primary production and accumulation of biomass (Gradinger, 2009). In impermeable ice, this flux is eliminated. However, the

694   algal biomass at SG was very low, even compared to other brackish sea ice system, such as the Baltic Sea with similar or lower

695   brine volume fractions and comparable light levels (Granskog et al., 2003: 3-6 mg Chl m^{-3}, Haecky & Andersson, 1999: 1.2

696   mg Chl m^{-2}), indicating that other stressors played a role at SG. Grazing is assumed to be a minor control on algae production

697   and biomass in Arctic sea ice (Gradinger, 2002). However, grazing by heterotrophic flagellates on small primary producers

698   has been described as important in the Baltic Sea, indicating that it might play a role at SG as well (Haecky & Andersson,

699   1999). SG sea ice communities were indeed dominated by small flagellate algae (microscopy based) and a high proportion of

700   potential grazers (18S rRNA data). Other stressors, such as phosphate limitation, viral lysis, or osmotic stress related to episodic

701   outbursts of subglacial meltwater are likely additional factors explaining the low biomass.

702   DIC has also been described as potentially limiting for sea ice primary production, especially towards the end of the bloom

703   (Haecky & Andersson, 1999) and may be supplied with the carbonate-rich subglacial outflow (Fransson et al., 2020). Higher

704   mortality due to factors mentioned above, together with the higher measured bacterial activity, allowing recycling of nutrients

705   may be a factor explaining higher production with lower Chl biomass. Lastly, nutrients may have been replenished recently

706   via advective processes when the brine volume fraction was higher.

707   At SG, another layer of potentially high activity has been found in the upper sea ice. In this layer, depleted nutrient

708   concentrations corresponded with high *Leptocylindrus minimus* abundances indicating that these algae were actively taking up

709   the nutrients, despite the impermeable sea ice. NO_X concentrations increased towards the surface and bottom indicating inputs

710   from surface flooding above (Granskog et al., 2003) and seawater below. Silicate and phosphate were only supplied from the

711   seawater below. The observed brine volume fractions below 5 % would not allow inputs of these nutrients, but episodes with

712   higher temperatures and thereby higher brine volume fractions may be sufficient to supply the needed nutrients to this

713   distinctive layer.

714   Overall, sea ice influenced by subglacial outflow was very similar to other brackish sea ice such as in the Baltic Sea concerning

715   structure, biomass and production (Haecky & Andersson, 1999, Granskog et al., 2005). Compared to Arctic sea ice, sea ice

22

716 algae biomass was reduced due to low brine volume fractions, phosphate limitation, and potentially higher mortality via grazing
717 and possibly higher osmotic stress.

5 Outlook

719 Our study showed that even a shallow marine-terminating glacier can lead to increased under-ice phytoplankton production
720 by locally enhanced light levels, stronger stratification and nutrient supply by subglacial discharge and upwelling, which are
721 all factors expected to change due to climate change. While much of our evidence is circumstantial, the number of different
722 lines of evidence leading to the same conclusion makes our findings rather robust. We propose that our findings are applicable
723 to other shallow tidewater glaciers with a polythermal or warm base, as is common on Svalbard (Hagen et al., 1993, Irvine-
724 Fynn et al., 2011). In the shorter term, a longer melt season and presumably increased subglacial discharge may lead to
725 increased subglacial upwelling in winter and spring. However, on longer time scales glaciers will retreat and transform towards
726 land-terminating glaciers (Błaszczyk et al., 2009), which would result in the lack of submarine discharge and systems more
727 similar to the NG and IE with less nutrients and light available for phytoplankton. The local effect would reduce primary
728 production, biomass and bacterial production in the water column, but would result in higher biomass of sea ice algae with the
729 known Arctic taxa of pennate diatoms. Considering the increased sedimentation rate at IE, we expect the pelagic/sympagic
730 benthic coupling to become stronger supporting the benthic food web. Winter and spring subglacial discharge is most likely
731 present at all polythermal or warm-based marine-terminating glaciers, which includes glacier termini with much deeper fronts,
732 much higher entrainment rates of bottom water, and higher silicate concentrations in the glacial meltwater (Hopwood et all.,
733 2020). Thus, the effect of early spring subglacial discharge is likely more pronounced in other fjords. Additional effects of
734 climate change include increased precipitation in the Arctic (Bintanja et al., 2020), which would reduce light levels below the
735 sea ice. However, also land-terminating glaciers would allow snow removal by katabatic winds as discussed for
736 Nordenskiöldbreen.

737 Another impact of climate change will be the reduction and earlier break-up of sea ice and Atlantification of fjords, leading to
738 increased light, and wind mixing. In the ice-free Kongsfjorden, higher primary production rates have been measured in the
739 same month, indicating that the lack of sea ice may lead to increased overall primary production (Iversen & Seuthe, 2010).
740 However, Kongsfjorden is still influenced by subglacial upwelling, supplying nutrients for the bloom (Halbach et al., 2017).
741 In systems not affected by subglacial upwelling the additional light will most likely not lead to substantially higher primary
742 production as indicated by lower measured rates in these type of fjords (Hopwood et al., 2020). Since the entrainment in our
743 study occurs at only approximately 20 m depth, upwelling under sea ice-free conditions would have much less effect, since
744 wind induced mixing plays a more important role. Direct silicate fertilisation would also have less effect in an ice-free fjord
745 since the fjord is likely more nitrate than silicate limited, due to the later stage of the spring bloom (Hegseth et al., 2019). In
746 summary, we suggest that subglacial upwelling in early spring is important for phytoplankton blooms, but only in a sea-ice
747 covered fjord. The future of the spring phytoplankton blooms depends on what happens first, disappearance of sea ice, or
748 retreat of the glacier to land.

6 Acknowledgements

7 Authors contributions

TRV designed the experiments, formulated the hypotheses and developed the sampling design with contributions of CD and UD, and RG. Fieldwork was conducted by TRV, UD, CD, EH, and JE with support by RG and EP for preparations. Lab analyses were done by TRV, UD, EP, CD, MC and EH. Computational analyses were performed by TRV. The manuscript has been prepared by TRV with contributions of all co-authors.

8 Data availability

Environmental data have been archived at Dataverse under the doi number https://doi.org/10.18710/MTPR9E. 18S and 16S rRNA sequences have been archived at the European Nucleotide archive under the project accession number PRJEB40294. The R and unix code for the statistical and bioinformatics analyses are available from the corresponding author upon request. More detailed reports of the fieldwork are available in the Research in Svalbard database under the RiS-ID 10889 (https://www.researchinsvalbard.no/project/7643). All maps (Fig. 1) were created using the PlotSvalbard R package (Vithakari, 2019). The Svalbard basemap is retrieved from the Norwegian Polar institute (2020, CC BY 4.0 license), the pan-Arctic map is retrieved from Natural Earth (2020, CC Public domain license), and the bathymetric map is retrieved from the Norwegian mapping authority (Kartverket, 2020, CC BY 4.0 license).

9 Competing interests

The authors declare that they have no conflict of interest.

References

Ambrožová, K., and Láska, K.: Air temperature variability in the vertical profile over the coastal area of Petuniabukta, central Spitsbergen, Polish Polar Research, 41-60, 2017.

Amundson, J. M., and Carroll, D.: Effect of topography on subglacial discharge and submarine melting during tidewater glacier retreat, Journal of Geophysical Research: Earth Surface, 123(1), 66-79, 2018.

Ardyna, M., Mundy, C. J., Mills, M. M., Oziel, L., Grondin, P. L., Lacour, L., Verin, G., Van Dijken, G., Ras, J., Alou-Font, E., Babin, M., Gosselin, M., Tremblay, J. É., Raimbault, P., Assmy, P., Nicolaus, M., Claustre, H. and Arrigo, K.R.: Environmental drivers of under-ice phytoplankton bloom dynamics in the Arctic Ocean, Elem Sci Anth, 8(1), 30, DOI: http://doi.org/10.1525/elementa.430, 2020.

Arrigo, K. R., Perovich, D. K., Pickart, R. S., Brown, Z. W., vanDijken, G. L., Lowry, K. E., Mills, M. M., Palmer, M. A., Balch,W. M., Bahr, F., Bates, N. R., Benitez-Nelson, C., Bowler, B.,Brownlee, E., Ehn, J. K., Frey, K. E., Garley, R., Laney, S.R., Lubelczyk, L., Mathis, J., Matsuoka, A., Mitchell, G. B.,Moore, G. W. K., Ortega-Retuerta, E., Pal, S., Polashenski, C.M., Reynolds, R. A., Schieber, B., Sosik, H. M., Stephens, M.,P., and Swift, J. H.: Massive phytoplankton blooms under Arctic sea ice, Science, 336, 1408, https://org/10.1126/science.1215065, 2012.

Arrigo, K. R., Arrigo, K. R., Perovich, D. K., Pickart, R. S., Brown, Z. W., van Dijken, G. L., Lowry, K. E., Mills, M. M., Palmer, M. A., Balch, W. M., Bates, N. R., Benitez-Nelson, C. R., Brownlee, E., Frey, K. E., Laney, S. R., Mathis, J., Matsuoka, A., Mitchell, B. G., Moore, G. W. K., Reynolds, R. A., Sosik, H. A., Swift, J. H.: Phytoplankton blooms beneath the sea ice in the Chukchi Sea, Deep Sea Res. Part II Top. Stud. Oceanogr., 105, 1-16, https://org/10.1016/j.dsr2.2014.03.018, 2014.

Arst, H., and Sipelgas, L.: In situ and satellite investigations of optical properties of the ice cover in the Baltic Sea region, in: Proceedings of the Estonian Academy of Sciences, Biology and Ecology, edited by: Aben, H., and Kurnitski, V., Estonian Academy of Sciences, Tallinn, 25-36, 2004.

Assmy, P., Ehn, J. K., Fernández-Méndez, M., Hop, H., Katlein, C., Sundfjord, A., Bluhm, K., Daaase, M., Engel, A., Fransson, A., Granskog, M. A., Hudson, S. R., Kristiansen, S., Nicolaus, M., Peeken, I., Renner, A. H. H., Spreen, G., Tatarek, A., and Wiktor, J.: Floating ice-algal aggregates below melting Arctic sea ice, PLoS ONE, 8(10), e76599, https://org/10.1371/journal.pone.0076599, 2013.

Assmy, P., M. Fernández-Méndez, P. Duarte, A. Meyer, A. Randelhoff, C. J. Mundy, L. M. Olsen, H. M. Kauko, A. Bailey,and Chierici, M.: Leads in Arctic pack ice enable early phytoplankton blooms below snow-covered sea ice,Scientific reports, 7, 40850, 2017.

Atienza, S., Guardiola, M., Præbel, K., Antich, A., Turon, X., and Wangensteen, O. S.: DNA Metabarcoding of Deep-Sea Sediment Communities Using COI: Community Assessment, Spatio-Temporal Patterns and Comparison with 18S rDNA, Diversity, 12(4), 123, https://org/10.3390/d12040123, 2020.

Azetsu-Scott, K., and Syvitski, J. P. M.: Influence of melting icebergs on distribution, characteristics and transport of marine particles in an East Greenland fjord, Journal of Geophysical Research 104 (C3), 5321–5328, 1999.

809 Bhatia, M. P., Kujawinski, E. B., Das, S. B., Breier, C. F., Henderson, P. B., and Charette, M. A.: Greenland meltwater as a
810 significant and potentially bioavailable source of iron to the ocean, Nat Geosci, 6(4), 274-278, https://org/10.1038/ngeo1746,
811 2013.

812 Bintanja, R., van der Wiel, K., Van der Linden, E. C., Reusen, J., Bogerd, L., Krikken, F., and Selten, F. M.: Strong future
813 increases in Arctic precipitation variability linked to 2226 poleward moisture transport, Sci. Adv., 6(7), eaax6869, 2020.

814 Błaszczyk, M., Jania, J. A., and Hagen, J. O.: Tidewater glaciers of Svalbard: Recent changes and estimates of calving fluxes,
815 Pol Polar Res, 2, 85-142, 2009.

816 Boyer, F., Mercier, C., Bonin, A., Le Bras, Y., Taberlet, P., and Coissac, E.: obitools: A unix-inspired software package for
817 DNA metabarcoding, Mol Ecol Resour, 16(1), 176-182, https://org/10.1111/1755-0998.12428, 2016.

818 Braaten, D. A.: A detailed assessment of snow accumulation in katabatic wind areas on the Ross Ice Shelf, Antarctica, J
819 Geophys Res Atmos, 102(D25), 30047-30058, https://org/10.1029/97JD02337, 1997.

820 Cantoni, C., Hopwood, M. J., Clarke, J. S., Chiggiato, J., Achterberg, E. P., and Cozzi, S.: Glacial drivers of marine
821 biogeochemistry indicate a future shift to more corrosive conditions in an Arctic fjord, Journal of Geophysical Research:
822 Biogeosciences, e2020JG005633, https://doi.org/https://doi.org/10.1029/2020JG005633, 2020.

823 Carroll, D., Sutherland, D. A., Hudson, B., Moon, T., Catania, G. A., Shroyer, E. L., Nash, J. D., Bartholomaus, T. C., Felikson,
824 D., Stearns, L. A., Noël, B. P. Y., and van den Broeke, M. R.: The impact of glacier geometry on meltwater plume structure
825 and submarine melt in Greenland fjords, Geophys. Res. Lett., 43, 9739–9748, https://doi.org/10.1002/2016GL070170, 2016.

826 Chandler, D. M., Wadham, J. L., Lis, G. P., Cowton, T., Sole, A., Bartholomew, I., Telling, J., Nienow, P., Bagshaw, E.B.,
827 Mair, D., Vinen, S., and Hubbard A.: Evolution of the subglacial drainage system beneath the Greenland Ice Sheet revealed
828 by tracers, Nat Geosci, 6(3), 195-198, https://org/10.1038/ngeo1737, 2013.

829 Christman, G. D., Cottrell, M. T., Popp, B. N., Gier, E., and Kirchman, D. L.: Abundance, diversity, and activity of ammonia-
830 oxidizing prokaryotes in the coastal Arctic Ocean in summer and winter, Appl. Environ. Microbiol., 77(6), 2026-2034,
831 https://org/10.1128/AEM.01907-10, 2011

832 Cloern, J. E., Grenz, C., and Vidergar-Lucas, L.: An empirical model of the phytoplankton chlorophyll: carbon ratio-the
833 conversion factor between productivity and growth rate, Limnol. Oceanogr., 40(7), 1313-1321,
834 https://org/10.4319/lo.1995.40.7.1313, 1995.

835 Cox, G. F., and Weeks, W. F.: Equations for determining the gas and brine volumes in sea-ice samples, J Glaciol, 29(102),
836 306-316, https://org/10.3189/S0022143000008364, 1983.

837 De Kluijver, A., Soetaert, K., Czerny, J., Schulz, K. G., Boxhammer, T., Riebesell, U., and Middelburg, J. J.: A 13C labelling
838 study on carbon fluxes in Arctic plankton communities under elevated CO_2 levels, Biogeosciences, 10(3), 1425-1440, 2013.

839 Dickson, A. G., Sabine, C. L., and Christian, J. R.: Guide to best practices for ocean CO_2 measurements, PICES Special
840 Publication 3, 2007.

841 Dowdeswell, J. A.: On the nature of Svalbard icebergs, J Glaciol, 35(120), 224-234, https://org/10.3189/S002214300000455X,
842 1989.

843 Egge, J. K., and Aksnes, D.L.: Silicate as regulating nutrient in phytoplankton competition, Mar Ecol Prog ser. Oldendorf, 83,
844 281-289, https://org/10.3354/meps083281, 1992.

845 Esau, I., and Repina, I.: Wind climate in Kongsfjorden, Svalbard, and attribution of leading wind driving mechanisms through
846 turbulence-resolving simulations, Advances in Meteorology, https://org/10.1155/2012/568454, 2012.

847 Fransson, A., Chierci, M., Nomura, D., Granskog, M. A., Kristiansen, S., Martma, T., and Nehrke, G.: Influence of glacialwater
848 and carbonate minerals on wintertime sea-ice biogeochemistry and the CO_2 system in an Arctic fjord in Svalbard, Annals of
849 Glaciology, 1–21, https://doi.org/10.1017/aog.2020.52, 2020.

850 Fransson, A., Chierci, M., Skjelvan, I., Olsen, A., Assmy, P., Peterson, A., Spreen, G., and Ward, B.: Effect of sea-ice and
851 biogeochemical processes and storms on under-ice water fCO_2 during the winter-spring transition in thehigh Arctic Ocean:
852 implications for sea-air CO_2 fluxes, J. Geophys. Res. Oceans, 122, 5566–5587, doi: 10.1002/2016JC012478, 2017.

853 Fofonoff, P., and Millard R. C.: Algorithms for computation of fundamental properties of seawater, Unesco Technical Papers
854 in Marine Science, 44, 53, http://hdl.handle.net/11329/109, 1983.

855 Fortier, M., Fortier, L., Michel, C., and Legendre, L.: Climatic and biological forcing of the vertical flux of biogenic particles
856 under seasonal Arctic sea ice, Mar. Ecol. Prog. Ser., 225, 1-16, https://org/10.3354/meps225001, 2002.

857 Furnas, M. J.: In situ growth rates of marine phytoplankton: approaches to measurement, community and species growth rate,
858 J Plankton Res, 12, 1117–1151, 1990.

859 Garrison, D. L., and Buck, K. R.: Organism losses during ice melting: a serious bias in sea ice community studies, Polar Biol
860 6:237-239, 1986.

861 Golden, K. M., Ackley, S. F., and Lytle, V. I.: The percolation phase transition in sea ice, Science, 282(5397), 2238-2241,
862 https://org/10.1126/science.282.5397.2238, 1998.

863 Gradinger, R.: Sea ice microorganisms, Encyclopedia of environmental microbiology, Wiley,
864 https://org/10.1002/0471263397.env310, 2003.

865 Gradinger, R.: Sea-ice algae: Major contributors to primary production and algal biomass in the Chukchi and Beaufort Seas
866 during May/June 2002, Deep Sea Res. Part II Top. Stud. Oceanogr., 56(17), 1201-1212,
867 https://org/10.1016/j.dsr2.2008.10.016, 2009.

868 Granskog, M. A., Kaartokallio, H., and Shirasawa, K.: Nutrient status of Baltic Sea ice: Evidence for control by snow-ice
869 formation, ice permeability, and ice algae, J Geophys Res Oceans, 108(C8), https://org/10.1029/2002JC001386, 2003.

870 Guardiola, M., Uriz, M. J., Taberlet, P., Coissac, E., Wangensteen, O. S., and Turon, X.: Deep-sea, deep-sequencing:
871 metabarcoding extracellular DNA from sediments of marine canyons, PloS one, 10(10), e0139633, 2015.

872 Haecky, P., and Andersson, A.: Primary and bacterial production in sea ice in the northern Baltic Sea, Aquat Microb Ecol,
873 20(2), 107-118, https://org/10.3354/ame020107, 1999.

874 Hagen, J. O., Liestøl, O., Roland, E., and Jørgensen, T.: Glacier Atlas of Svalbard and Jan Mayen, Oslo: Norwegian Polar
875 Institute, 1993.

876 Halbach, L., Vihtakari, M., Duarte, P., Everett, A., Granskog, M. A., Hop, H., Kauko, H. M., Kristiansen, S., Myhre, P. I.,
877 Pavlov, A. K., Pramanik, A., Tatarek, A., Torsvik, T., Wiktor, J. M., Wold, A., Wulff, A., Steen, H., Assmy, P.: Tidewater
878 glaciers and bedrock characteristics control the phytoplankton growth environment in a fjord in the arctic, Front Mar Sci, 6,
879 254, https://org/10.3389/fmars.2019.00254, 2019.

880 Hatton, J. E., Hendry, K. R., Hawkings, J. R., Wadham, J. L., Kohler, T. J., Stibal, M., Beaton, A. D., Bagshaw, E. A., and
881 Telling, J.: Investigation of subglacial weathering under the Greenland Ice Sheet using silicon isotopes, Geochim Cosmochim
882 Acta, 247, 191-206, https://org/10.1016/j.gca.2018.12.033, 2019.

883 Hawkings, J. R., Wadham, J. L., Benning, L. G., Hendry, K. R., Tranter, M., Tedstone, A., Nienow, P., and Raiswell, R.: Ice
884 sheets as a missing source of silica to the polar oceans, Nat. Commun, 8(1), 1-10, https://org/10.1038/ncomms14198, 2017.

885 Hegseth, E. N., Assmy, P., Wiktor, J. M., Wiktor, J., Kristiansen, S., Leu, E., Tverberg, V., Gabrielsen, T. M., Skogseth, R.,
886 and Cottier, F.: Phytoplankton seasonal dynamics in Kongsfjorden, Svalbard and the adjacent shelf, in: The Ecosystem of
887 Kongsfjorden, Svalbard, edited by: Hop, H., and Wiencke, C., Springer, Cham., 173-227, 2019.

888 Hodal, H., Falk-Petersen, S., Hop, H., Kristiansen, S., and Reigstad, M.: Spring bloom dynamics in Kongsfjorden, Svalbard:
889 nutrients, phytoplankton, protozoans and primary production, Polar Biol 35, 191–203, https://doi.org/10.1007/s00300-011-
890 1053-7, 2012.

891 Hodgkins, R.: Glacier hydrology in Svalbard, Norwegian high arctic, Quat Sci Rev, 16(9), 957-973, https://org/10.1016/S0277-
892 3791(97)00032-2, 1997.

893 Holmes, F. A., Kirchner, N., Kuttenkeuler, J., Krützfeldt, J., and Noormets, R.: Relating ocean temperatures to frontal ablation
894 rates at Svalbard tidewater glaciers: Insights from glacier proximal datasets, Sci. Rep, 9(1), 1-11, https://org/10.1038/s41598-
895 019-45077-3, 2019.

896 Hopwood, M. J., Carroll, D., Dunse, T., Hodson, A., Holding, J. M., Iriarte, J. L., Ribeiro, S., Achterberg, E. P., Cantoni, C.,
897 Carlson, D. F., Chierici, M., Clarke, J. S., Cozzi, S., Fransson, A., Juul-Pedersen, T., Winding, M. S. and Meire, L.: How does
898 glacier discharge affect marine biogeochemistry and primary production in the Arctic?, Cryosphere, 14, 1347-1383, https://org/
899 10.5194/tc-14-1347-2020, 2020.

900 Irvine-Fynn, T. D., Hodson, A. J., Moorman, B. J., Vatne, G., & Hubbard, A. L.: Polythermal glacier hydrology: A review,
901 Reviews of Geophysics, 49(4), 2011.

902 Iversen, K. R., and Seuthe, L.: Seasonal microbial processes in a high-latitude fjord (Kongsfjorden, Svalbard): I. Heterotrophic
903 bacteria, picoplankton and nanoflagellates, Polar Biol, 34(5), 731-749, https://org/10.1007/s00300-010-0929-2, 2011.

904 Jones, E., Chierici, M., Skjelvan, I., Norli, M., Børsheim, K. Y., Lødemel, H. H., Sørensen, K., King, A. L., Lauvset, S.,
905 Jackson, K., de Lange, T., Johannsessen, T., and Mourgues, C.: Monitoring ocean acidification in Norwegian seas in 2018,
906 Miljødirektoratet, M-1417|2019, 2019.

907 Kanna, N., Sugiyama, S., Ohashi, Y., Sakakibara, D., Fukamachi, Y., and Nomura, D.: Upwelling of macronutrients and
908 dissolved inorganic carbon by a subglacial freshwater driven plume in Bowdoin Fjord, northwestern Greenland, J Geophys
909 Res Biogeosci, 123(5), 1666-1682, https://org/10.1029/2017JG004248, 2018.

910   Kartverket, https://kartkatalog.geonorge.no/metadata/kartverket/dybdedata/2751aacf-5472-4850-a208-3532a51c529a, last

911   access: 10 August 2020.

912   Kirchman, D. L., Malmstrom, R. R., and Cottrell, M. T.: Control of bacterial growth by temperature and organic matter in the

913   Western Arctic, Deep Sea Research Part II: Topical Studies in Oceanography, 52(24-26), 3386-3395, 2005.

914   Kowalik, Z., Marchenko, A., Brazhnikov, D., and Marchenko, N.: Tidal currents in the western Svalbard Fjords, Oceanologia,

915   57(4), 318-327, https://org/10.1016/j.oceano.2015.06.003, 2015.

916   Krisch, S., Browning, T. J., Graeve, M., Ludwichowski, K.U., Lodeiro, P., Hopwood, M. J., Roig, S., Yong, J. C., Kanzow,

917   T., and Achterberg, E. P.: The Influence of Arctic Fe and Atlantic Fixed N on Summertime Primary Production in Fram Strait,

918   North Greenland Sea, Sci. Rep, 10 (1), 15230, https://doi.org/10.1038/s41598-020-72100-9, 2020.

919   Leppäranta, M., and Manninen, T.: The brine and gas content of sea ice with attention to low salinities and high temperatures,

920   Finnish Institute of Marine Research Internal Report, 2, 1-15, 1988.

921   Láska, K., Witoszová, D., and Prošek, P.: Weather patterns of the coastal zone of Petuniabukta, central Spitsbergen in the

922   period 2008–2010, Polish Polar Research, 297-318, 2012.

923   Leu, E., Mundy, C. J., Assmy, P., Campbell, K., Gabrielsen, T. M., Gosselin, M., Juul-Pedersen, T., and Gradinger, R.: Arctic

924   spring awakening–Steering principles behind the phenology of vernal ice algal blooms, Prog Oceanogr, 139, 151-170,

925   https://org/10.1016/j.pocean.2015.07.012, 2015.

926   Lowry, K. E., Pickart, R. S., Selz, V., Mills, M. M., Pacini, A., Lewis, K. M., Joy-Warren, H., Nobre, C., van Dijken, G. L.,

927   Grondin, P., Ferland, J., and Arrigo, K. R.: Under-ice phytoplankton blooms inhibited by spring convective mixing in

928   refreezing leads, J Geophys Res Oceans, 123(1), 90-109, https://org/10.1002/2016JC012575, 2018.

929   Lydersen, C., Assmy, P., Falk-Petersen, S., Kohler, J., Kovacs, K. M., Reigstad, M., Stehen, H., Strøm, H., Sundfjord, A.,

930   Varpe, Ø., Walczowski, W., Weslawski, K. M., and Zajaczkowski, M.: The importance of tidewater glaciers for marine

931   mammals and seabirds in Svalbard, Norway, J Marine Sys, 129, 452-471, https://org/10.1016/j.jmarsys.2013.09.006, 2014.

932   Maes, S.: Polar cod population structure: connectivity in a changing ecosystem, Ph.D. thesis, KU Leuven, Leuven, Belgium,

933   2017.

934   Mahé, F., Rognes, T., Quince, C., de Vargas, C., and Dunthorn, M.: Swarm: robust and fast clustering method for amplicon-

935   based studies, PeerJ, 2, e593, https://org/10.7717/peerj.593, 2014

936   Massicotte, P., Bécu, G., Lambert-Girard, S., Leymarie, E., and Babin, M.: Estimating underwater light regime under spatially

937   heterogeneous sea ice in the Arctic, Appl. Sci., 8(12), 2693, https://org/10.3390/app8122693, 2018.

938   Meire, L., Meire, P., Struyf, E., Krawczyk, D. W., Arendt, K. E., Yde, J. C., Juul Pedersen, T., Hopwood, M. J., Rysgaard, S.,

939   and Meysman, F. J. R.: High export of dissolved silica from the Greenland Ice Sheet, Geophys. Res. Lett., 43, 9173–9182,

940   https://doi.org/10.1002/2016GL070191, 2016a.

941   Meire, L., Mortensen, J., Rysgaard, S., Bendtsen, J., Boone, W., Meire, P., and Meysman, F. J.: Spring bloom dynamics in a

942   subarctic fjord influenced by tidewater outlet glaciers (Godthåbsfjord, SW Greenland), J Geophys Res Biogeosci, 121(6),

943   1581-1592, https://org/10.1002/2015JG003240, 2016b.

944 Meslard, F., Bourrin, F., Many, G., and Kerhervé, P.: Suspended particle dynamics and fluxes in an Arctic fjord (Kongsfjorden,

945 Svalbard), Estuarine, Estuar Coast Shelf S, 204, 212-224, https://org/10.1016/j.ecss.2018.02.020, 2018.

946 Mortensen, J., Rysgaard, S., Bendtsen, J., Lennert, K., Kanzow, T., Lund, H., and Meire, L.: Subglacial Discharge and Its

947 Down-Fjord Transformation in West Greenland Fjords With an Ice Mélange, J Geophys Res Oceans, 125(9), e2020JC016301,

948 2020.

949 Moskalik, M., Ćwiąkała, J., Szczuciński, W., Dominiczak, A., Głowacki, O., Wojtysiak, K., and Zagórski, P: Spatiotemporal

950 changes in the concentration and composition of suspended particulate matter in front of Hansbreen, a tidewater glacier in

951 Svalbard, Oceanologia, 60(4), 446-463 2018.

952 Mock, T., and Gradinger, R.: Determination of Arctic ice algal production with a new in situ incubation technique, Mar. Ecol.

953 Prog. Ser., 177, 15-26, https://org/10.3354/meps177015, 1999.

954 Molari, M., Manini, E., and Dell'Anno, A.: Dark inorganic carbon fixation sustains the functioning of benthic deep-sea

955 ecosystems, Global Biogeochem Cycles, 27(1), 212-221, https://org/10.1002/gbc.20030, 2013.

956 Moon, T., Sutherland, D. A., Carroll, D., Felikson, D., Kehrl, L., and Straneo, F.: Subsurface iceberg melt key to Greenland

957 fjord freshwater budget, Nat Geosci, 11(1), 49-54, https://org/10.1038/s41561-017-0018-z, 2018.

958 Mundy, C. J., Barber, D. G., and Michel, C.: Variability of snow and ice thermal, physical and optical properties pertinent to

959 sea ice algae biomass during spring, J Marine Sys, 58(3-4), 107-120, https://org/10.1016/j.jmarsys.2005.07.003, 2005.

960 Mundy, C. J., Gosselin, M., Ehn, J., Gratton, Y., Rossnagel, A., Barber, D. G., Martin, J., Tremblay, J., Palmer, M., Arrigo,

961 K. R., Darnis, G., Fortier, L., Else, B., Papakyriokou, T.: Contribution of under-ice primary production to an ice-edge upwelling

962 phytoplankton bloom in the Canadian Beaufort Sea, Geophys. Res. Lett, 36(17), https://org/10.1029/2009GL038837, 2009.

963 Natural Earth, http://www.naturalearthdata.com/, last access: 10 August 2020.

964 Norwegian Polar institute, Toposvalbard, https://toposvalbard.npolar.no, last access: 16 Septemper 2020.

965 Pabi, S., van Dijken, G. L., and Arrigo, K. R.: Primary production in the Arctic Ocean, 1998–2006, J Geophys Res Oceans,

966 113(C8), https://org/10.1029/2007JC004578, 2008.

967 Parada, A. E., Needham, D. M., and Fuhrman, J. A.: Every base matters: assessing small subunit rRNA primers for marine

968 microbiomes with mock communities, time series and global field samples, Environ. Microbiol, 18(5), 1403-1414,

969 https://org/10.1111/1462-2920.13023, 2016.

970 Parsons, T. R., Maita, Y. and Lalli, C. M. (Eds.): A Manual of Chemical and Biological Methods for Seawater Analysis.

971 Pergamon Press, Toronto, 1984.

972 Pavlov, A. K., Leu, E., Hanelt, D., Bartsch, I., Karsten, U., Hudson, S. R., Gallet, J., Cottier, F., Cohen, J. H., Berge, J.,

973 Johnsen, G., Maturilli, M., Kowalczuk, P., Sagan, S., Meler, J., and Granskog, M. A.: The underwater light climate in

974 Kongsfjorden and its ecological implications, in: The Ecosystem of Kongsfjorden, Svalbard, edited by: Hop, H., and Wiencke,

975 C., Springer, Cham., 137-170, 2019.

976 Perovich, D. K., Roesler, C. S., and Pegau, W. S.: Variability in Arctic sea ice optical properties, J Geophys Res Oceans,

977 103(C1), 1193-1208, https://org/10.1029/97JC01614, 1998.

978   Porter, K. G., and Feig, Y. S.: The use of DAPI for identifying and counting aquatic microflora1, Limnol Oceanogr, 25, 943–

979   948, https://wiley.com/10.4319/lo.1980.25.5.0943, 1980.

980   Pruesse, E., Peplies, J., and Glöckner, F. O.: SINA: accurate high-throughput multiple sequence alignment of ribosomal RNA

981   genes, Bioinformatics, 28(14), 1823-1829, 2012.

982   Ptacnik, R., Andersen, T., and Tamminen, T.: Performance of the Redfield ratio and a family of nutrient limitation indicators

983   as thresholds for phytoplankton N vs. P limitation, Ecosystems, 13(8), 1201-1214, https://org/10.1007/s10021-010-9380-z,

984   2010.

985   Quast, C., Pruesse, E., Yilmaz, P., Gerken, J., Schweer, T., Yarza, P., Replies, J., and Glöckner, F. O.: The SILVA ribosomal

986   RNA gene database project: improved data processing and web-based tools. Nucleic acids research, 41(D1), D590-D596,

987   2012.

988   Redfield, A. C.: On the proportions of organic derivatives in sea water and their relation to the composition of plankton, In

989   James Johnstone Memorial Volume, 176–192. Liverpool University Press, 1934.

990   Rich, J., Gosselin, M., Sherr, E., Sherr, B., and Kirchman, D. L.: High bacterial production, uptake and concentrations of

991   dissolved organic matter in the Central Arctic Ocean, Deep Sea Research Part II: Topical Studies in Oceanography, 44(8),

992   1645-1663, 1997.

993   Sager, J. C., and Mc Farlane, J. C.: Radiation, in: Plant growth chamber handbook, edited by: Langhans, R. W., and Tibbits,

994   T. W., Iowa Agr. Home Econ. Expt. Sta. Special Rpt, 99, 1-29, 1997.

995   Schaffer, J., and Kanzow, T.: von Appen, W. J.; von Albedyll, L.; Arndt, J. E.; Roberts, D. H. Bathymetry Constrains Ocean

996   Heat Supply to Greenland's Largest Glacier Tongue, Nat. Geosci, 13(3), 227-231, https://doi.org/10.1038/s41561-019-0529-

997   x, 2020.

998   Schoof, C., Rada, C. A., Wilson, N. J., Flowers, G. E., and Haseloff, M.: Oscillatory subglacial drainage in the absence of

999   surface melt, The Cryosphere, 8(3), 959-976, 2014.

1000   Skogseth, R., Olivier, L. L., Nilsen, F., Falck, E., Fraser, N., Tverberg, V., Ledang, A. B., Vader, A., Jonassen, M. O., Søreide,

1001   J., Cottier, F., Berge, J., Ivanov, B. V., and Falk-Petersen, S.: Variability and decadal trends in the Isfjorden (Svalbard) ocean

1002   climate and circulation-an indicator for climate change in the European Arctic, Prog Oceanogr, 187, 102394,

1003   https://org/10.1016/j.pocean.2020.102394, 2020.

1004   Southwood, T. R. E. and Henderson, P. A. (Eds.): Ecological methods, John Wiley and Sons, 269, 2000.

1005   Strzelecki, M. C.: Schmidt hammer tests across a recently deglacierized rocky coastal zone in Spitsbergen-is there a "coastal

1006   amplification" of rock weathering in polar climates?, Pol Polar Res, 239-252, https://org/10.2478/v10183−011−0017−5, 2011.

1007   Sutherland, D. A., Pickart, R. S., Peter Jones, E., Azetsu-Scott, K., Jane Eert, A., and Ólafsson, J.: Freshwater composition of

1008   the waters off southeast Greenland and their link to the Arctic Ocean, J Geophys Res Oceans, 114(C5),

1009   https://org/10.1029/2008JC004808, 2009.

1010   Sutherland, D. A., Straneo, F., & Pickart, R. S.: Characteristics and dynamics of two major Greenland glacial fjords, Journal

1011   of Geophysical Research: Oceans, 119(6), 3767-3791, 2014.

1012 Throndsen, J., Hasle, G. R., & Tangen, K. (Eds.): Phytoplankton of Norwegian coastal waters, Almater Forlag AS, 2007.

1013 Tomas, C. R. (Ed.): Identifying Marine Phytoplankton, Elsevier, San Diego, 1997.

1014 Utermöhl, H.: Methods of collecting plankton for various purposes are discussed, SIL Commun 1953-1996. 9, 1–38,
1015 https://doi.org/10.1080/05384680.1958.11904091, 1958.

1016 Van De Poll, W. H.; Kulk, G.; Rozema, P. D.; Brussaard, C. P. D.; Visser, R. J. W.; Buma, A. G. J. Contrasting Glacial
1017 Meltwater Effects on Post-Bloom Phytoplankton on Temporal and Spatial Scales in Kongsfjorden, Spitsbergen, Elementa,
1018 https://doi.org/10.1525/elementa.307, 2018.

1019 Vihtakari, M.: PlotSvalbard: PlotSvalbard - Plot research data from Svalbard on maps. R package version 0.9.2,
1020 https://github.com/MikkoVihtakari/PlotSvalbard, 2020.

1021 von Quillfeldt, C. H.: Common diatom species in Arctic spring blooms: their distribution and abundance, Bot Mar, 43(6), 499-
1022 516, https://org/10.1515/BOT.2000.050, 2000.

1023 von Quillfeldt, C. H., Ambrose, W. G., and Clough, L. M.: High number of diatom species in first-year ice from the Chukchi
1024 Sea, Polar Biol, 26(12), 806-818, https://org/10.1007/s00300-003-0549-1, 2003.

1025 Vonnahme, T. R., Devetter, M., Žárský, J. D., Šabacká, M., and Elster, J.: Controls on microalgal community structures in
1026 cryoconite holes upon high Arctic glaciers, Svalbard, Biogeosciences, 13, 659-674, https://org/10.5194/bg-13-659-2016, 2016.

1027 Wadham, J. L., Hodgkins, R., Cooper, R. J., and Tranter, M.: Evidence for seasonal subglacial outburst events at a polythermal
1028 glacier, Finsterwalderbreen, Svalbard, Hydrol. Process., 15(12), 2259-2280, https://org/10.1002/hyp.178, 2001.

1029 Wang, Q., Garrity, G. M., Tiedje, J. M., and Cole, J. R.: Naive Bayesian Classifier for Rapid Assignment of rRNA Sequences
1030 into the New Bacterial Taxonomy, Appl Environ Microbiol. 73(16), 5261-7, https://org/ 10.1128/AEM.00062-07, 2007.

1031 Wangensteen, O. S., Palacín, C., Guardiola, M., and Turon, X.: DNA metabarcoding of littoral hard-bottom communities: high
1032 diversity and database gaps revealed by two molecular markers, PeerJ, 6, e4705, https://org/10.7717/peerj.4705, 2018.

1033 Wiedmann, I., Reigstad, M., Marquardt, M., Vader, A., and Gabrielsen, T. M.: Seasonality of vertical flux and sinking particle
1034 characteristics in an ice-free high arctic fjord—Different from subarctic fjords?, J Marine Sys, 154, 192-205,
1035 https://org/10.1016/j.jmarsys.2015.10.003, 2016.

1036 Wilson, N.: Characterization and interpretation of polythermal structure in two subarctic glaciers, Doctoral dissertation,
1037 Science: Department of Earth Sciences, 2012.

1038 Wynn, P. M., Hodson, A. J., Heaton, T. H., and Chenery, S. R.: Nitrate production beneath a High Arctic glacier, Svalbard,
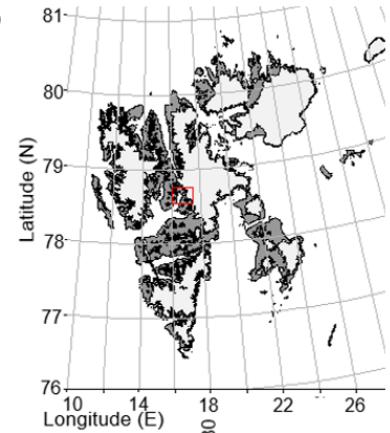1039 Chemical geology, 244(1-2), 88-102, 2007.

1040 yr.no,   Longyearbyen   –   historikk,   https://www.yr.no/nb/historikk/graf/1-
1041 2759929/Norge/Svalbard/Svalbard/Longyearbyen?q=2019-04, last access: 24 July 2020.

1042

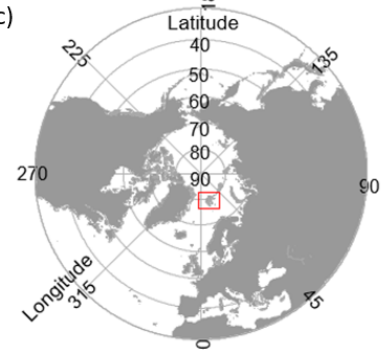1043

1044

1045

Figures
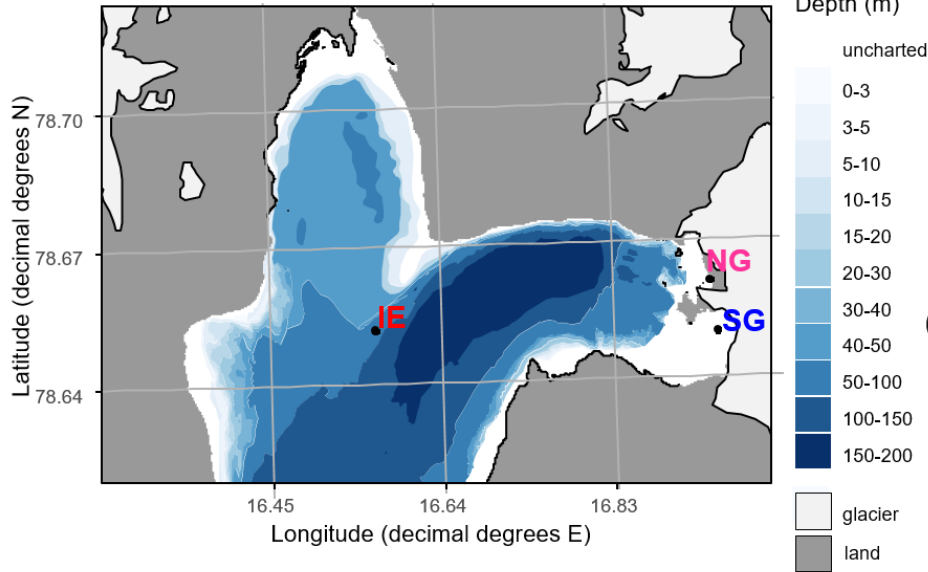
1049 Fig 1. Sampling sites in Billefjorden: a) detailed Billefjorden map showing the stations at the ice edge (IE), north glacier (NG)
1050 and south glacier (SG) on the underlying bathymetric map. White areas are uncharted with water depths of about 30 m at NG
1051 and SG. The insets to the right show the location of b) Billefjorden on a Svalbard map and of c) Svalbard on a pan-Arctic map,
1052 marked with red boxes. Land is shown as dark grey, ocean as white, and glaciers as light grey.
1053
1054

1055
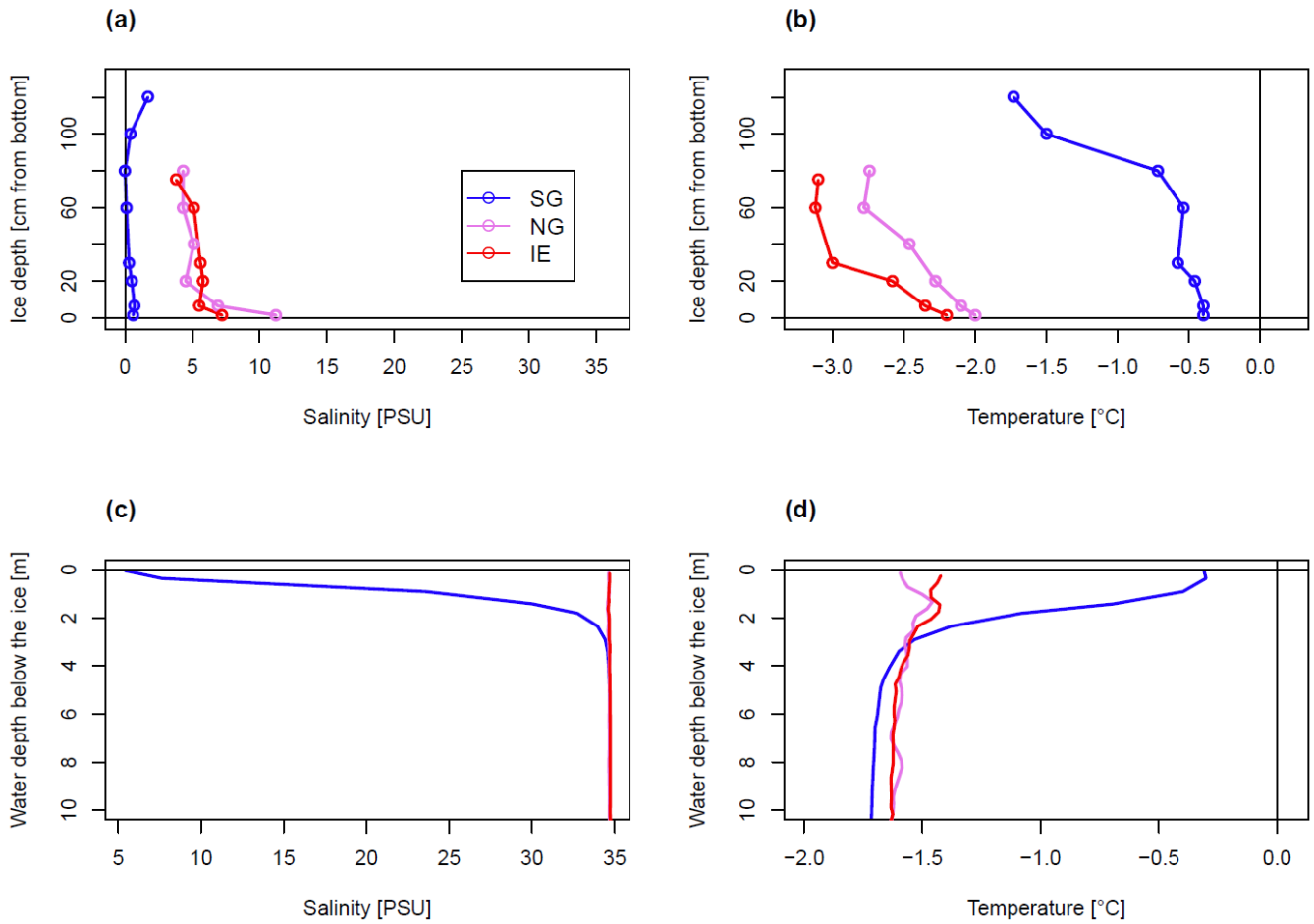
Fig 2. Bulk salinity and temperature profiles in a,b) sea ice cores (0 cm at the bottom) and c,d) the water column down to 10 m below the sea ice, of the three stations.
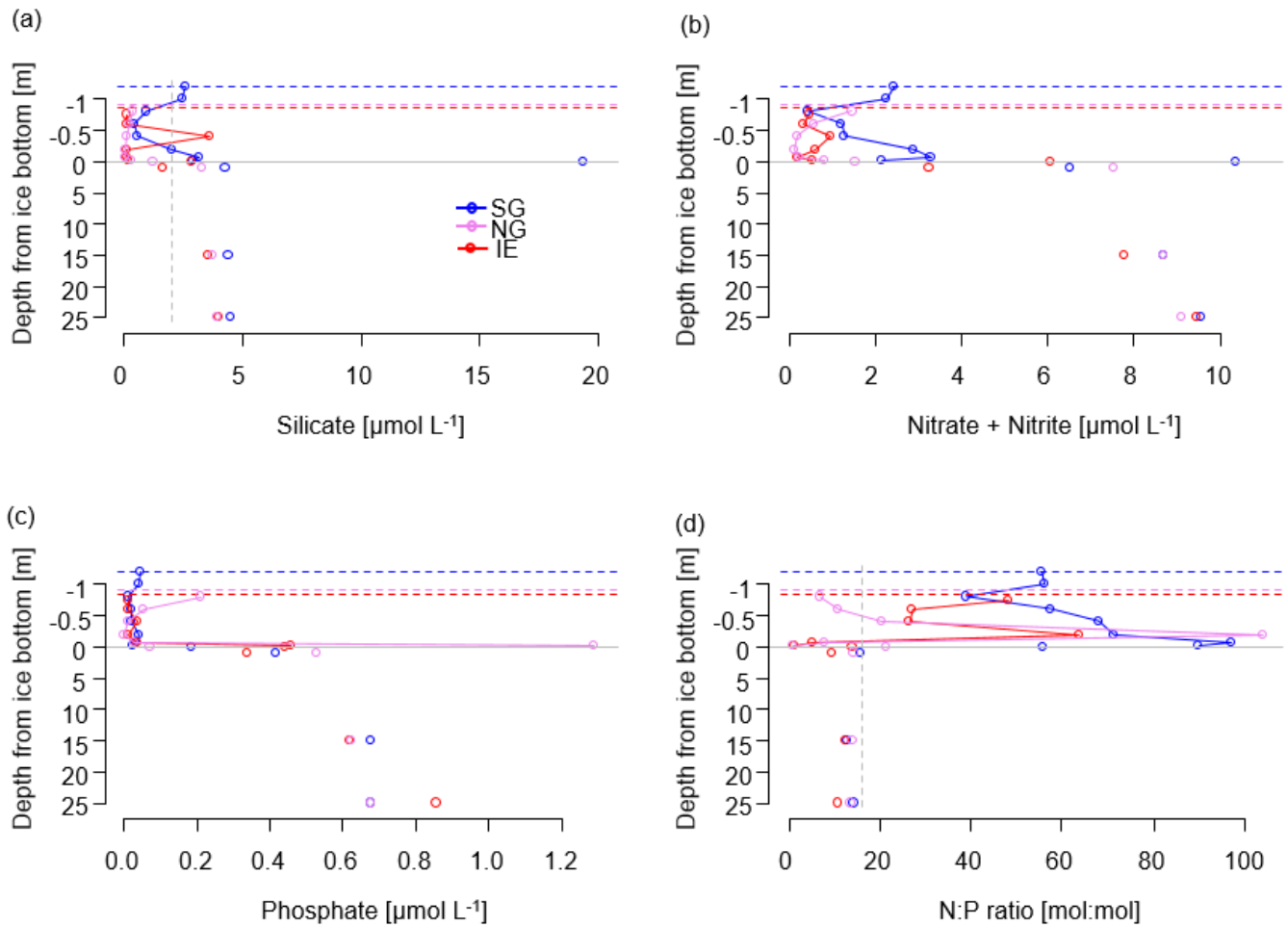
1056
1057
1058
1059
1060
1061
1062
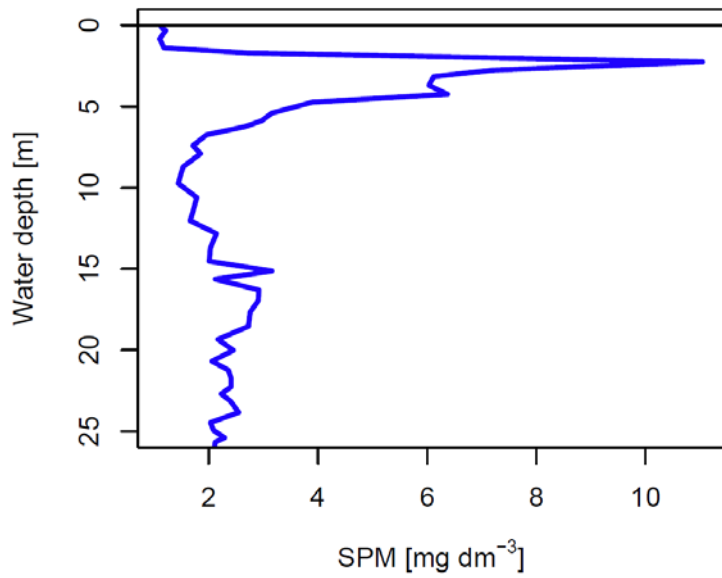
34

Fig 3. Turbidity profile of the SG station converted to suspended particles.

Fig 4. Nutrients in the water column (below grey line) and in sea ice (above the grey line) of a) silicate with a suggested threshold for limitation marked as dashed grey line, b) NO_X as nitrate and nitrite, c) phosphate and d) molar N:P ratios with the Redfield threshold of N:P 16:1 marked as dashed grey line indicating potential N limitation. Dashed lines indicate the position of the ice surface, while solid lines show the measured data.
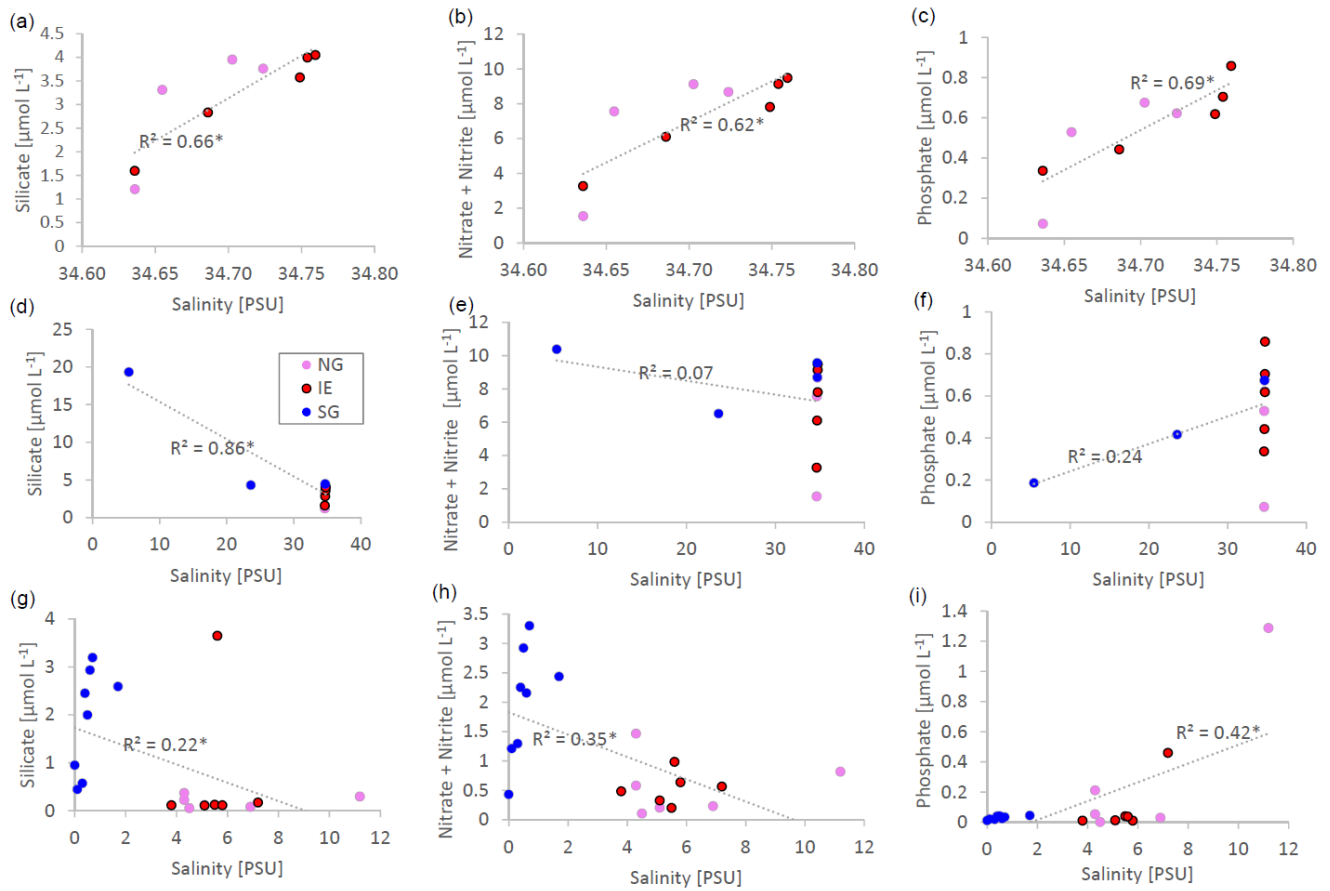
1077

1078 Fig 5. Linear salinity-nutrient correlations of NG and IE water samples (a–c), NG, IE, and SG water stations (d–f) and sea ice

1079 samples of NG, IE and SG (bulk salinities) (g–i). A higher concentration in saline Atlantic water is shown as a positive

1080 correlation, a higher concentration in glacial meltwater as a negative correlation. Significant correlations (p<0.05) are asterisk

1081 marked behind the R^2 value.

1082
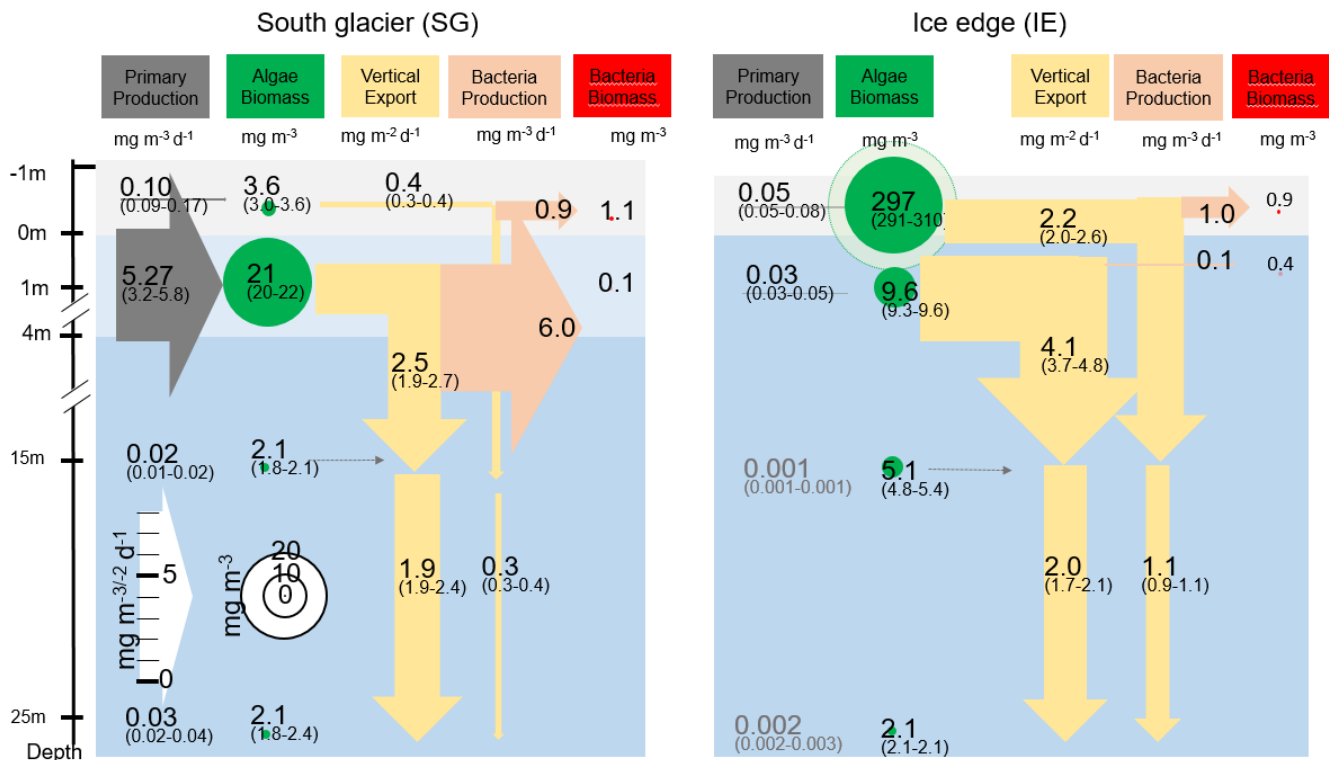
Fig 6. Schematic representation of the C cycle at SG and IE stations. All units are in mg C with the median given in the circles and arrows and the minimum and maximum in brackets below. 0 m depth is at the sea ice water interface. Grey arrows indicate net primary production with its height scaled to the uptake rates. Green circles show standing stock algae biomass converted from Chl to C (conversion factor = 30 gC gChl[-1], Cloern et al., 1995) with its diameter scaled to the concentrations, except sea ice at IE with the light green circle scaled one order of magnitude higher. Yellow arrows indicate vertical export of chlorophyll converted to C (conversion factor = 30 gC gChl[-1], Cloern et al., 1995) with the contribution of sea ice algae and phytoplankton estimated by the fraction of typical sea ice algae in phytoplankton net hauls and the width of the arrows scaled to the fluxes. Orange arrows indicate bacterial biomass production based on dark carbon fixation (conversion factor = 129 gC gDIC[-1], Molari et al., 2013) with the arrows scaled to the values. Red circles to the right are bacteria biomass assuming 20 fg C cell[-1] in the bottom sea ice and UIW. The grey area represents sea ice, the light blue area a brackish water layer and the darker blue area deeper saline water layers.
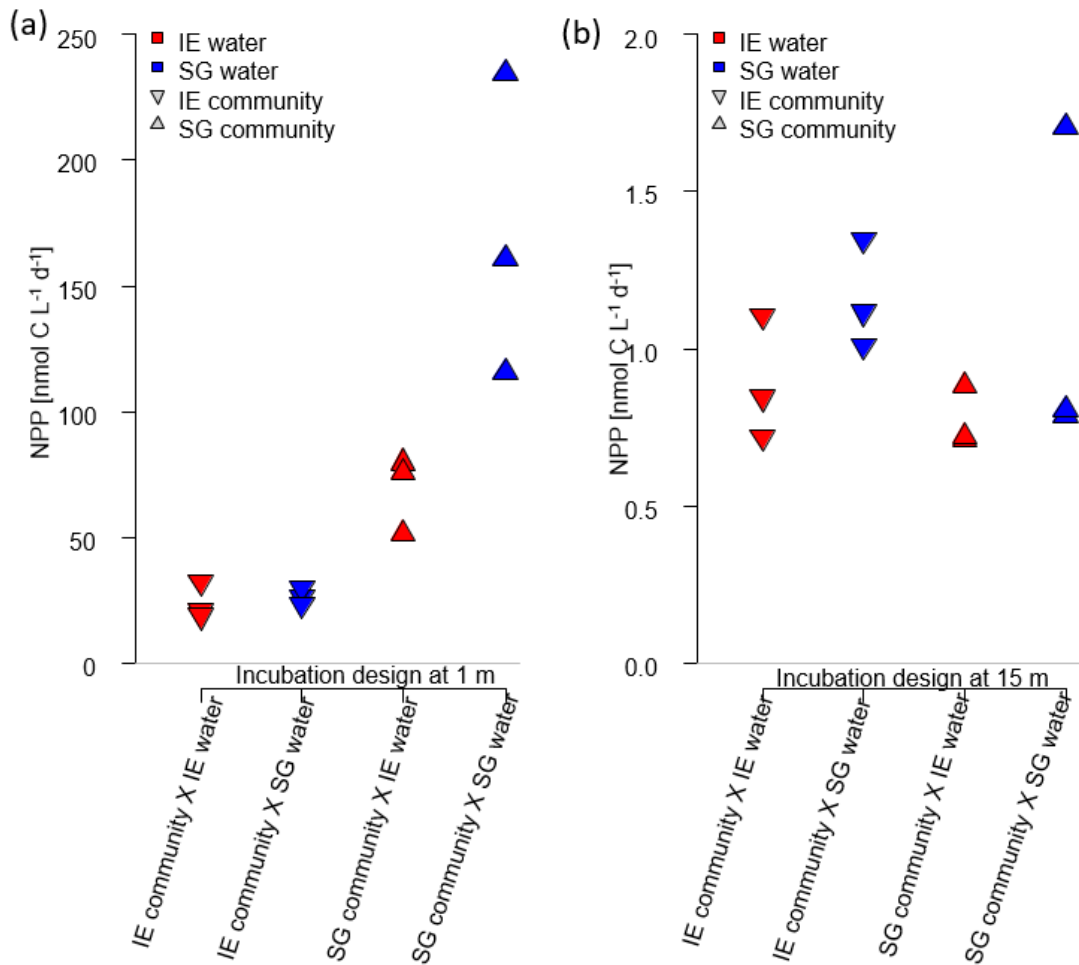
1097

1098 Fig 7. Impact of water source on primary production assessed via a reciprocal transplant experiment. Primary production of

1099 IE and SG communities incubated in sterile filtered water originated from either station at a) 1 m and b) 15 m depth. The

1100 symbols show the source of the community and the colors indicate the source of the sterile filtered incubation water. The type

1101 of incubation water (color) explains the variation in a nested ANOVA with community (symbol) and depth as nested

1102 constrained variables and water source (color) as explanatory variable (p=0.0038, F=10.88).

1103
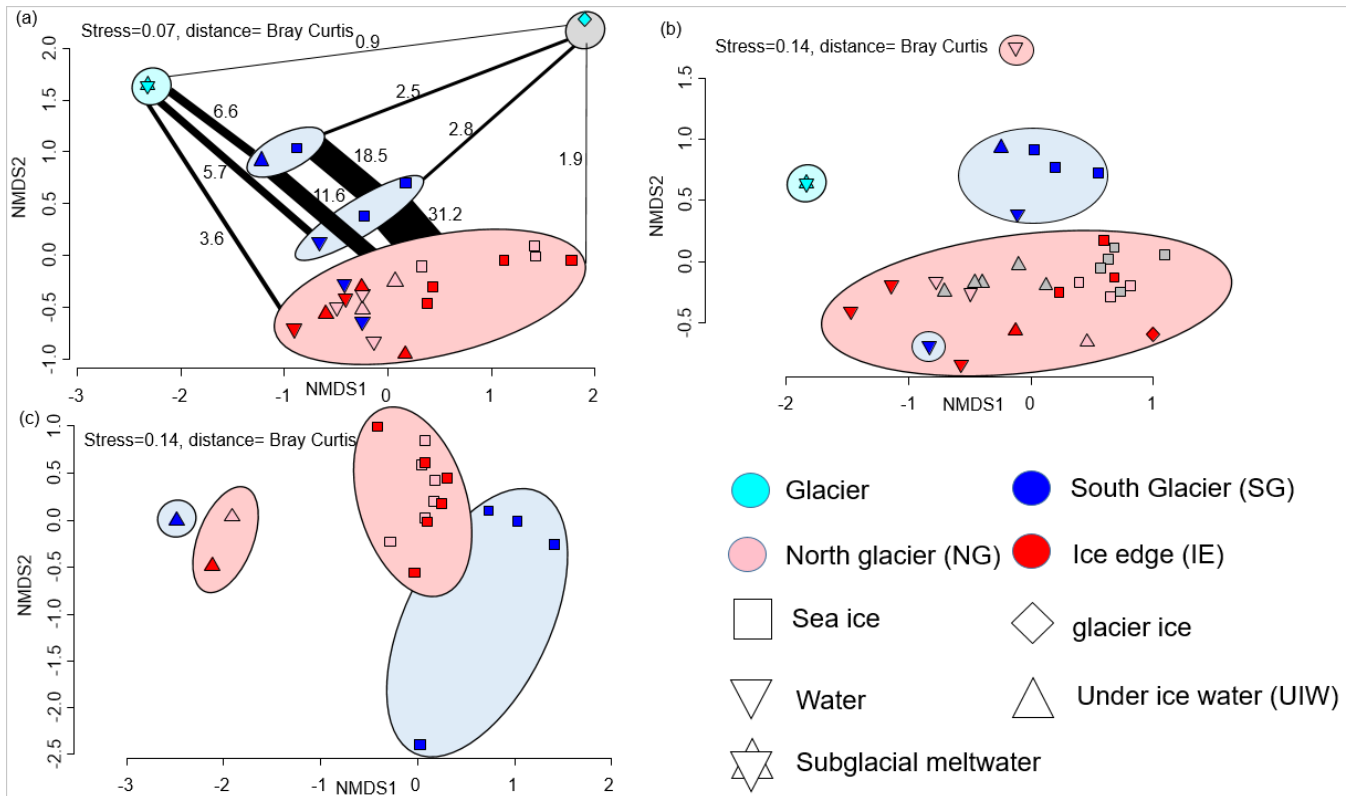
1106 Fig 8. a) NMDS plot of microbial community structure based on 16S data (stress = 0.07), including samples from April 2018.

1107 Groups highlighted in eclipses: glacier ice (top right in grey eclipse), undiluted subglacial outflow (top left in cyan eclipse),

1108 surface samples (UIW, sea ice) at station SG 2019 (top blue eclipse), surface samples (1m water, sea ice) at station SG 2018

1109 (bottom blue eclipse) and others including deeper water samples at SG (bottom in red eclipse). The fraction of shared OTUs

1110 (in %) are shown as lines scaled to the fraction [%] of shared OTUs. b) NMDS plot of community structure based on 18S data

1111 (stress = 0.14), including samples from April 2018 with the surface water sample of NG as outlier on top, and a surface water

1112 sample of SG as outlier in the pink reference cluster, c) NMDS plot based on algae abundances in sea ice and UIW based on

1113 light microscopic counts (stress = 0.14).

1114

1115

1116

1117

1118

1119

1120

Tables

Table 1. Properties of 1) marine surface and 2) marine deep water (both station IE), 3) subglacial discharge melt water and 4) station SG surface water and the relative contribution of the water types 1 to 3 to form water type 4. The calculations are given in the Supplement and are based on different salinities and nutrients in the 4 water masses.

	1) Surface water (IE 1 m)		2) Bottom water (IE)		3) Subglacial discharge meltwater		4) SG (1 m)
Salinity [PSU]	34.7		34.7		0	32 ± 0.1 %	23.6
Temperature [°C]	-1.4		-1.4		0		-0.4
Silicate [μmol L^{-1}]	1.59	0 %	4.46	> 84 %	1.79	32 %	4.30
NO_X [μmol L^{-1}]	3.27	10 ± 3 %	9.57	58 ± 1 %	2.06	32 %	6.52
Phosphate [μmol L^{-1}]	0.34	19 ± 3 %	0.67	49 ± 3 %	0.09	32 %	0.42

1146 Table 2. Integrated standing stock biomass of Chl and fluxes of Chl and C, fractions of the different fluxes and standing stocks,

1147 and bacterial production based on dark carbon fixation (DCF).

Variable	SG	IE	Unit
Chl integrated in sea ice	0.02	0.40	mg m^{-2}
NPP in bottom sea ice	0.10	0.05	mg C m^{-3} d^{-1}
Chl integrated in 25 m water column	3.74	3.75	mg m^{-2}
Vertical Chl flux to 25 m	0.07	0.11	mg Chl m^{-2} d^{-1}
NPP at 1 m	5.27	0.03	mg C m^{-3} d^{-1}
C based NPP int. over 25 m	42.6	0.2	mg C m^{-2} d^{-1}
Estimated Chl production int. over 25 m	1.4	0.0	mg C m^{-2} d^{-1}
mg C fixed per mg Chl	11.4	0.1	mg C mg Chl d^{-1}
NPP as fraction of Chl standing stock	38 %	0.2 %	% Chl renewal d^{-1}
Doubling time	2.63	500	days
Vertical Chl flux as % of Chl standing stock	2 %	3 %	% export of Chl d^{-1}
Vertical Chl flux as % of NPP based Chl prod.	5 %	1375 %	% export of NPP d^{-1}
Loss of Chl from 15 to 25 m	12 %	19 %	Δexp 15m to 25m
Average Chl fraction of (Chl + Phaeo) in 0-3 cm ice	30%	85%	% Chl
Average Chl fraction of (Chl + Phaeo) in water	47 %	50 %	% Chl
Bacteria DCF ice	7.0	7.6	µg C m^{-3} d^{-1}
Bacteria Biomass prod (DCF based) ice	0.9	1.0	mg C m^{-3} d^{-1}
Doubling time	1.2	0.9	days
Bacteria DCF 1 m	46.9	1.1	µg DIC m^{-3} d^{-1}
Bacteria Biomass prod (DCF based) 1m	6.0	0.1	mg C m^{-3} d^{-1}
Doubling time	0.02	2.9	days

1148

1149

1150

1151

1152

1153

1154

1155

1156

Appendix

Equations 1-6. Mixing calculations for estimates of the fraction of meltwater (MW_{Sal}) based on salinity, and for bottom water based on nutrient concentrations (BW_{Nuts}). Sal indicates the average salinities measured at the IE (Sal_{IE}), SG at 1m depth (Sal_{SG1m}), subglacial outflow (Sal_{glac}). Nut indicates the nutrient concentrations of nitrate and nitrite (NO_X), silicate (Si), and phosphate (PO4) at 1m under the sea ice at SG (Nut_{1mSG}) and IE (Nut_{1mIE}), the bottom water of the IE (Nut_{BW}), or subglacial outflow water (Nut_{glac}).

$$MW_{Sal}[\%] = \frac{Sal_{IE} - Sal_{SG1m}}{Sal_{SG1m} - Sal_{glac} + Sal_{IE} - Sal_{SG1m}} * 100 \tag{1}$$

$$MW_{Sal}[\%] = \frac{34.7\ PSU - 23.6\ PSU}{23.6\ PSU - 0\ PSU + 34.7\ PSU - 23.6 PSU} * 100 = 32\ \% \tag{2}$$

$$BW_{Nut}[\%] = \frac{Nut_{1mSG} - MW_{Sal}[\%] * Nut_{glac} - Nut_{1m_{IE}} + MW_{Sal}[\%] * Nut_{1m_{IE}}}{Nut_{BW} - Nut_{1m_{IE}}} * 100 \tag{3}$$

$$BW_{NOX}[\%] = \frac{6.52\mu M - 0.32 * 2.06\ \mu M - 3.27\ \mu M + 0.32 * 3.27\ \mu M}{9.57\ \mu M - 3.27\ \mu M} * 100 = 58\ \% \tag{4}$$

$$BW_{Si}[\%] = \frac{4.30\ \mu M - 0.32 * 1.79\ \mu M - 1.59\ \mu M + 0.32 * 1.59\ \mu M}{4.46\ \mu M - 1.59\ \mu M} * 100 = 92\ \% \tag{5}$$

$$BW_{PO4}[\%] = \frac{0.41\ \mu M - 0.32 * 0.09\ \mu M - 0.34\ \mu M + 0.32 * 0.34\ \mu M}{0.67\ \mu M - 0.34\ \mu M} * 100 = 46\ \% \tag{6}$$

Equation 7. Calculation of vertical flux of Chl based on the sediment traps with concentration of Chl (C), Volume in the sediment trap cylinder (V), area above the cylinder (A) and incubation time (t).

$$Vertical\ flux = \frac{C * V}{A * t} \tag{7}$$